Reversing protonation of weakly basic drugs greatly enhances intracellular diffusion and decreases lysosomal sequestration

Debabrata Dey,[1] Shir Marciano,[1] Anna Poryvai,[2] Ondřej Groborz,[2] Lucie Wohlrábová,[2] Tomás Slanina,[2] and Gideon Schreiber*,[1]

[1]Department of Biomolecular Sciences, Weizmann Institute of Science, Israel

[2]Institute of Organic Chemistry and Biochemistry of the Czech Academy of Sciences, Flemingovo náměstí 542/2, Prague 6, 160 00 Czech Republic

*Corresponding author: gideon.schreiber@weizmann.ac.il

KEYWORDS: Small molecule drugs, diffusion, in-cell, lysosome

ABSTRACT: Drug efficacy depends not only on delivery but also on intracellular diffusion, distribution and availability. Yet, more than a half of pharmaceutical drugs are weakly basic and thus, protonated and sequestered at intracellular pH. Protonation reduces their diffusion rates due to macromolecular crowding and nonspecific interactions, and subcellular sequestration prevents them from reaching their target due to ion trapping. Here, we explored the intracellular diffusion rates of a series of small molecular fluorescent drugs by fluorescence recovery after the photobleaching (FRAP). We found a strong correlation between drug pK_a and intracellular diffusion and distribution. Weakly basic, small-molecule drugs displayed slower fraction recovery after photobleaching and 10-to-20-fold lower diffusion rates in cells than in aqueous solutions, suggesting sequestration. But while our imaging studies showed that acidic organelles, particularly the lysosome, captured these molecules, blocking lysosomal import did not improve diffusion. Instead, blocking protonation enhanced their diffusion, as shown by their *N*-acetylated analogues. Moreover, co-administration with basic quinacrine, which is accumulated in lysozymes, prevented the sequestration of the anti-cancer drug mitoxantrone, thereby improving its biodistribution. Based on these results, combining *N*-acetylation with co-administration may improve the intracellular diffusion and distribution of weakly basic, small molecule drugs.

INTRODUCTION

Small molecules are essential for most cellular activities.[1–3] Due to their easiness of administration, bioactivity, stability and scaling of production, most drugs are small molecules (< 1 kDa).[4,5] Over a half of these drugs have significant degree of hydrophobicity and are weakly basic at intracellular pH of 7.2.[6,7] Hydrophobicity helps the drug molecule to cross the lipid bilayer of the cell membranes, and polar functional groups help to solubilize the drug into the cellular medium.[7] The balance between pK_a and logP is critical for successful drug design.[8,9] For a long time, passive diffusion[10] and carrier-mediated drug delivery[11] or a combination of both[12] have been postulated to explain intracellular drug delivery. However,

transport of a drug across the cellular membrane is only one part of the successful delivery. Intracellular diffusion and bio-distribution needs to be taken in account when assessing the drug mode of action.

In previous work, we studied the diffusion behavior of fluorescent drug molecules under crowding conditions constituting proteins and polymers, thus, mimicking the cellular environment.[13] However, the cellular cytoplasm of eukaryotic cells is by far more complex than can be mimicked *in vitro*.[14] This relates to the presence of intracellular membranes, multiple organelles,[15,16] and large diversity of macromolecules, in terms of size, charge and hydrophobicity of the cellular milieu.[17,18] Moreover, the pH inside cellular organelles can vastly differ from the cytosolic.[19] Organelles like lysosomes, late endosomes, Golgi, and secretory vesicles are acidic and have been known for sequestering weakly basic drugs.[20,21] Therefore, predicting diffusion of a particular drug molecule in the dense cytoplasm is a complex task.

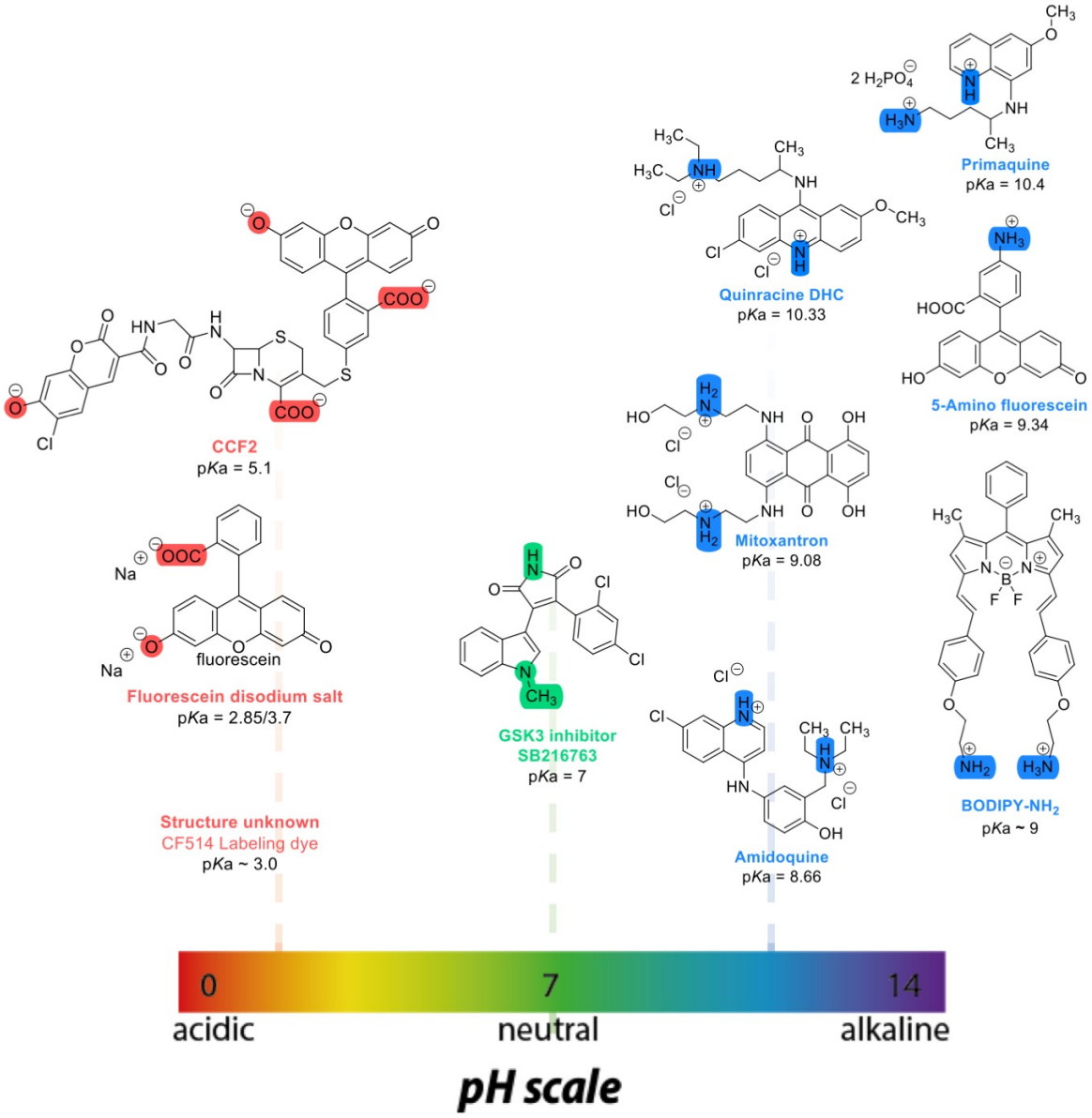

Figure 1. Chemical structures and p*K*a values (prediction from ChemAxon software) of the small molecules and drugs used in this study.

For example, drugs that are designed to target the DNA in the nucleus (and thus are basic),[22,23] may bind cytoplasmic materials through non-specific interactions, be sequestrated within the lysosome, or diffuse slower than expected due to crowding or non-specific interactions.[24–26]

Monitoring diffusion behavior is a good proxy for predicting intracellular drug delivery and other processes, such as non-specific binding or aggregation.[13] The primary tool for measuring cellular diffusion is fluorescence recovery after the photobleaching (FRAP), which inherently requires all studied molecules to be fluorescent. FRAP under a confocal microscope is a sensitive versatile method that is suitable for measurement of weakly fluorescent molecules, as opposed to single molecules fluorescence correlation spectroscopy.[13,27,28]

In this work, we investigated intracellular diffusion of a series of fluorescent dyes and drugs (Figure 1 and Table 1) by FRAP. For most measurements we used Line-FRAP, which has a much lower death time and faster data accumulation in comparison to standard FRAP (800 Hz versus 50 Hz, for detailed

Table 1: LogP, pKa and lysosomal sequestration of drugs used in this study (Predicted by ChemAxon software, and obtained from drug bank data base[26])

Therapeutic Indication	Drug/Small Molecules	Calculated LogP	Calculated p*K*a (Strongest basic)	Lysosomal sequestration
Anti-cancer	mitoxantrone	1.19	9.08	+
Anti-Malarial	quinacrine	5.15	10.33	+
	primaquine-biphosphate	1.64	10.4	+
	amodiaquine	4.83	8.66	+
Other Small molecules	5-Amino fluorescein	3.02	9.34	+
	fluorescein-Sodium Salt	2.65	2.85/3.7	-
	BODIPY-NH_2	_	9.00	_
	BODIPY-NHAc	_	_	_
	CCF2	_	5.1	_
	CF514	_	~3.0 (from UV spectrum)	_

Values of p*K*a were estimated using ChemAxon. Lysosomal sequestration was taken from the in cell micrographs in this work.

explanations see ref [13] and [28]). We studied the following drugs with intrinsic fluorescence in the visible spectrum: the antimalarial drugs quinacrine dihydrochloride,[29] primaquine phosphate[30] and amidoquine;[31] the anti-cancer drug mitoxantrone;[32] the glycogen synthase kinase GSK3 inhibitor SB216763.[33] In addition, we monitored the diffusion of the diagnostic staining agent fluorescein disodium salt,[34] the fluorogenic substrate CCF2[35] and boron dipyrromethene (BODIPY) analogues, which are used as fluorescent markers for lipids, membranes, and other lipophilic compounds.[36]

Measuring the diffusion coefficients of these compounds and their cellular distributions showed very slow diffusion of the basic compounds, low FRAP recovery and accumulation in lysosomes. Surprisingly, while inhibiting the V-ATPase H^+ pump using Bafilomycin A1[37,38] or sodium azide[39] did indeed inhibit accumulation in lysosomes, it did not increase the cellular diffusion of these compounds or their fraction recovery. Contrary, blocking protonatable amino groups by acetylation greatly enhanced diffusion and FRAP recovery of studied small molecules. As over half the small molecule drugs are basic, our findings are of high importance in future drug development, as slow diffusion and low FRAP recovery is directly related with reduced activity in the cell.

RESULTS

Negatively charged fluorescein, CCF2 and CF514 rapidly diffuse in live cells. Fluorescein is an organic small molecule (M.W. = 332 Da, Figure 1) that is negatively charged (pK_a's = 2.85, 3.7, Table 1). In previous work, we have shown that fluorescein diffusion is slowed by adding proteins, even at relatively low concentrations.[13] Here, we measured the diffusion coefficients of fluorescein in the cytoplasm of live HeLa cells, observing almost complete recovery from photobleaching within 1s (Figure 2A-C). $D_{confocal}$ of 56 $\mu m^2 s^{-1}$ in PBS was reduced to $D_{confocal}$ 38 $\mu m^2 s^{-1}$ in the crowded cellular cytoplasm of HeLa cells (Figure 2B). In the cell nucleus, a value of $D_{confocal}$ of 42 $\mu m^2 s^{-1}$ was determined, while in concentrated HeLa cell extract (equivalent protein concentration of ~100 mg/mL), $D_{confocal}$ of 48 $\mu m^2 s^{-1}$ was measured. The faster $D_{confocal}$ in cell extract compared to live-cell cytoplasm may result from the higher crowding density of the latter. The lowering of diffusion coefficients of negatively charged fluorescein correlates with the increasing crowding density of the medium moving from simple buffer to cells. Fluorescein dye was micro-injected in live HeLa cells, with FRAP measurements following directly after. For comparison, we incubated HeLa cells for 24 h with fluorescein (which is the sufficient time for fluorescein to accumulate in HeLa cells by diffusion). While micrographs did not show dye aggregation inside the cell cytoplasm (Figure S1A-B) and diffusion rates are the same as determined by microinjection (Figure S1C and S1D), the fraction recovery dropped from 0.95 to 0.65. This would suggest that a fraction of fluorescein aggregated in the cell after 24 h incubation.

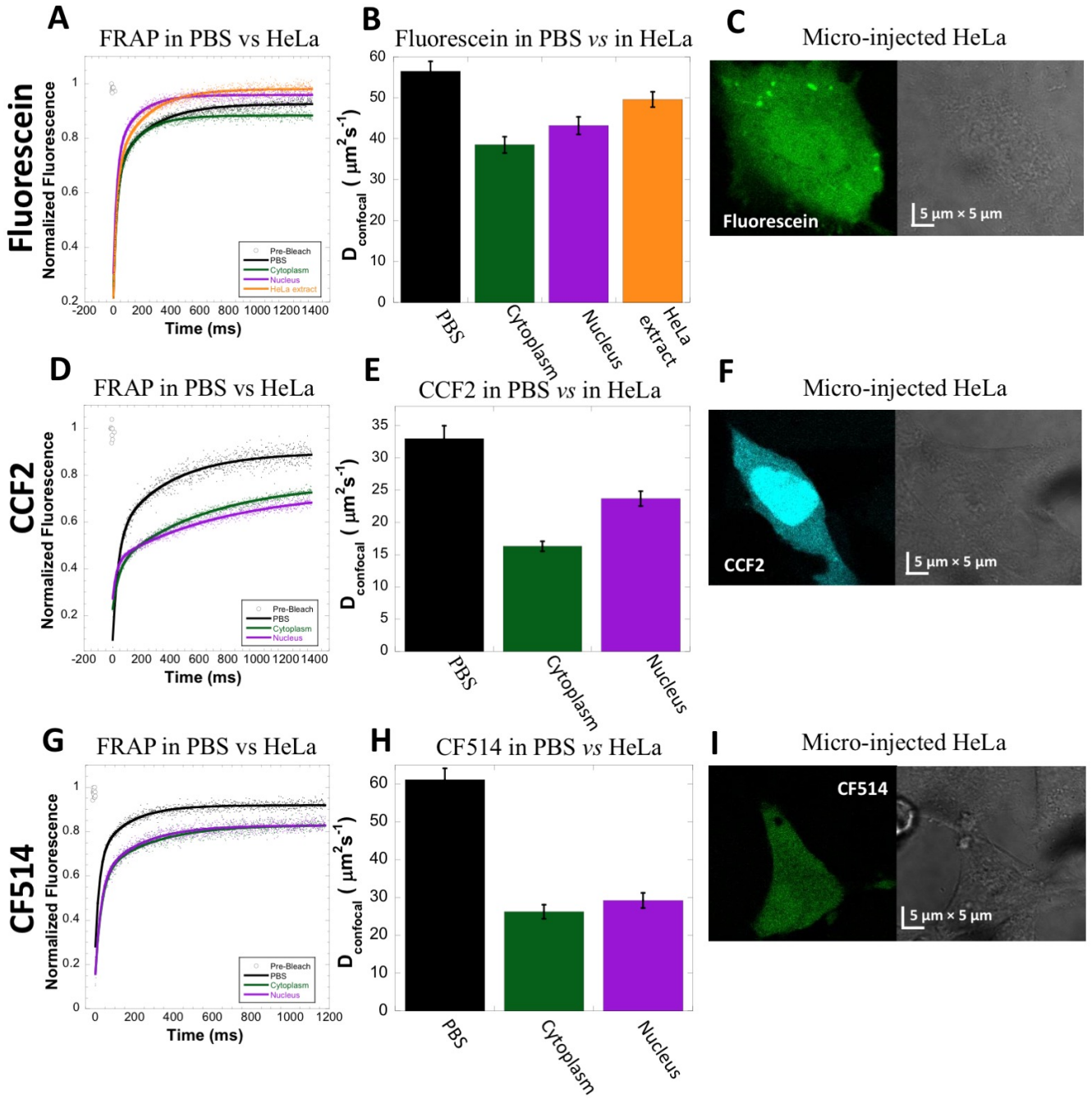

Figure 2. Fluorescein, CCF2 and CF514 diffusion in PBS and inside HeLa cells. Comparative FRAP profiles in PBS and inside HeLa cells with exponential fits are shown for (A) Fluorescein and (D) CCF2 and (G) CF514. Comparative $D_{confocal}$ values for (B) Fluorescein (E) CCF2 and (H) CF514 are also shown. Micro-injected HeLa cells are shown in (C) for Fluorescein (F) for CCF2 and (I) for CF514 dye.

CCF2 is a fluorogenic substrate used for monitoring β-lactamase activity. It is composed of cephalosporin core linking B7-hydroxycoumarin to fluorescein (Figure 1). Its calculated $D_{confocal}$ values are ~1/2 of those measured for fluorescein (Figure 2D-F) in PBS and inside cells. At least partially, this could be explained by its higher MW (856 Da, versus 332 Da for fluorescein). Both parts of CCF2 are weak acids, with no sign of aggregation seen in micrographs inside the cell cytoplasm or nucleus (Figure 2F).

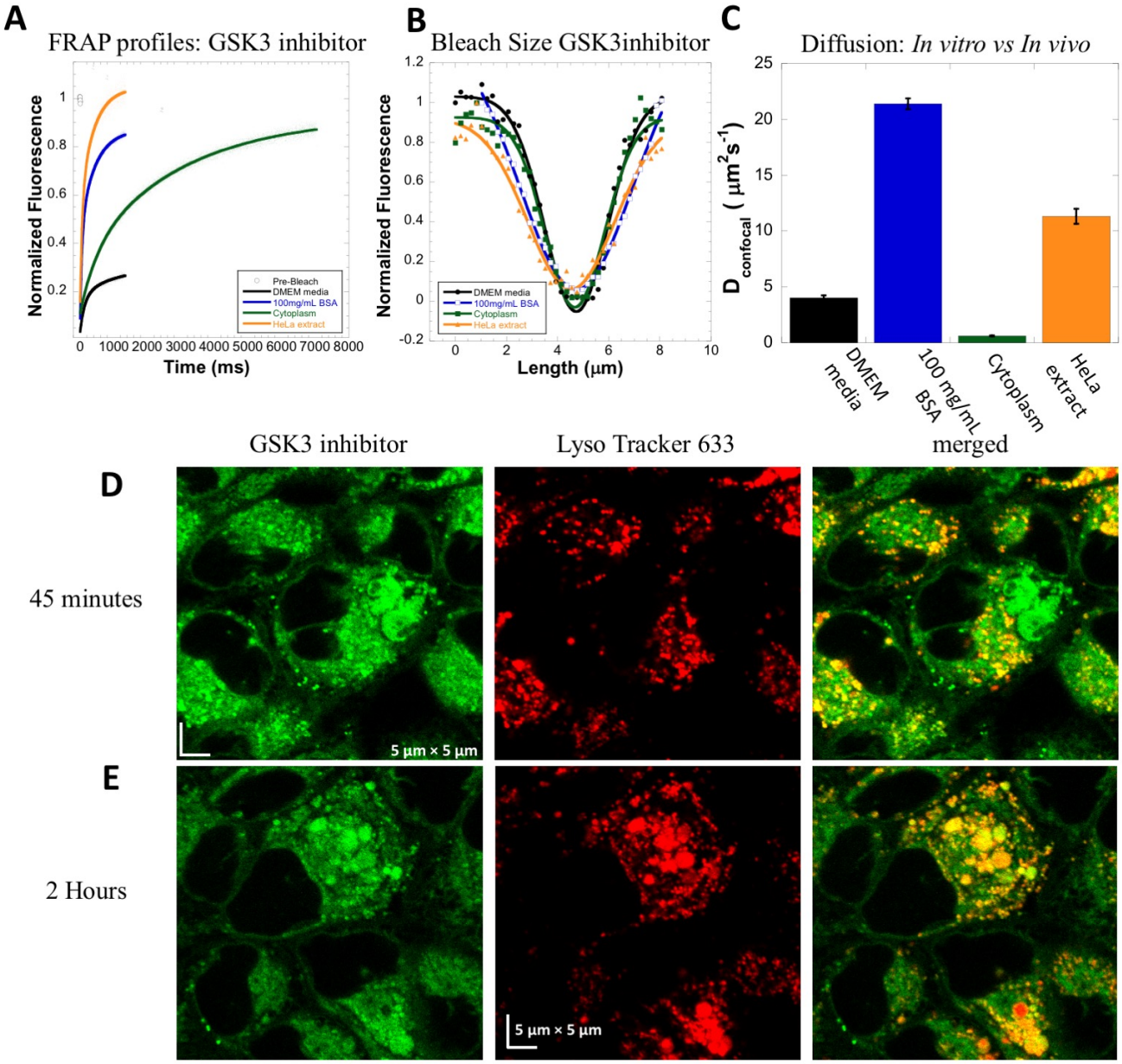

Figure 3. Diffusion of GSK3 inhibitor in PBS and inside HeLa cells. Comparative (A) FRAP recovery profiles with exponential fits for GSK3 inhibitor (SB216763), (B) Averaged bleach size profiles with gaussian fits, and (C) Diffusion coefficients in PBS buffer, in 50 mg/mL of BSA, HeLa cell extract and in HeLa cells are shown. (D-E) Colocalization of GSK3 inhibitor in lysosomal compartments are shown. HeLa cells were treated with Lyso Tracker 633 for 30 mins. GSK3 inhibitor treatment for (D) 45 mins and (E) 2 hours respectively at 10 µM concentrations are also shown.

A third molecule for which we determined the diffusion coefficient is CF514. It is used to label proteins and has high quantum yield. As its structure has not been published, we estimated the pK_a value from the pH dependent UV-spectrophotometry measurements. The sharp changes of the UV- spectrum at pH~3 (Figure S1E-F), as well as the redshift confirms a pK_a value of ~ 3. The FRAP curves look similar to fluorescein (Figure 2G-I) with ~90% recovery after FRAP. $D_{confocal}$ in PBS was ~ 61 $\mu m^2 s^{-1}$, and 26 and

29 $\mu m^2 s^{-1}$ in the cell cytoplasm and nucleus of HeLa cells respectively (Figure 2H). The drop of $D_{confocal}$ is attributed to cellular crowding.

High FRAP recovery but slow diffusion measured for the GSK3 inhibitor SB216763. The GSK3 inhibitor SB216763 (M.W.=371 Da, Figure 1) aggregates when dissolved in PBS buffer, which can be reversed by adding BSA.[13] Comparative FRAP profiles and $D_{confocal}$ rates of SB216763 in different mediums are shown in Figure 3A-C. For comparison to live cell cytoplasm, we used 100 mg/mL of BSA or DMEM media. The FRAP profiles and relative $D_{confocal}$ values show very slow diffusion of SB216763 in HeLa cell cytoplasm of ~0.61 $\mu m^2 s^{-1}$ (Figure 3A). This is a 40-fold reduction compared to measurements in 100 mg/mL BSA protein solution ($D_{confocal}$~24.3 $\mu m^2 s^{-1}$). In DMEM media (containing 5% serum protein) FRAP recovery was also very slow, indicating that the drug is still aggregating.[13] Interestingly, the $D_{confocal}$ value in HeLa cell extract was higher ~ 11.3 $\mu m^2 s^{-1}$ and its fraction recovery was high (0.9 versus <0.3 in DMEM medium), showing that HeLa cell extract, like BSA is disaggregating SB216763. Micrographs of HeLa cells show aggregation of SB216763 in the cytoplasm. Co-localization with Lysotracker-633 (Figure 3D-E) shows that SB216763 colocalizes and is sequestered in acidic chambers of the cell lysosomes. Moreover, SB216763 aggregation into the lysosome increased over time (Figure 3D and E, 45-minute and 2 h treatment). Varying drug dosages resulted in $D_{confocal}$ values of 0.42-0.61 $\mu m^2 s^{-1}$, suggesting that the slow diffusion is not related to SB216763 concentration (Figure S2A-B).

Despite the high solubility of Quinacrine, its diffusion in HeLa cells is slow. Quinacrine DHC (M.W.= 472.9 Da, Figure 1) is a compound highly soluble in PBS,[13] with a fast $D_{confocal}$ rate of 41.9 $\mu m^2 s^{-1}$ (Figure 4A-C). This rate dropped to $D_{confocal}$~2.45 $\mu m^2 s^{-1}$ in HeLa cell cytoplasm, with fraction recovery of ~0.8, in comparison to 1 in buffer. In HeLa cell extract a $D_{confocal}$ rate of 15.1 $\mu m^2 s^{-1}$ was determined, which lays between PBS and HeLa cytoplasm. Micrographs of live HeLa cells show that the quinacrine DHC molecules aggregate in the cytoplasm. Co-localization with Lysotracker-633 (Figure 4D-E) shows that quinacrine colocalizes and is sequestered in acidic chambers of the cell lysosomes. Moreover, quinacrine aggregation into the lysosome increased over time (Figure 4D and E, 45-minute and 2 h treatment). Quinacrine is accumulating over time within the lysosome. Therefore, we measured diffusion instantaneously following micro-injection, and compared it to 2 and 24 h of incubation (Figure S3A-B). But, as quinacrine accumulates rapidly in the lysosome, it is observed even instantaneously after micro-injection with increasing aggregation at longer times. $D_{confocal}$ of 4.2 $\mu m^2 s^{-1}$ was calculated from line-FRAP instantaneously after micro-injection, slowing to 2.2 $\mu m^2 s^{-1}$ following 2 hours incubations. After 24 hours incubation the fraction recovery is less than 25%, and thus the diffusion value is meaningless (Figure S3C and D).

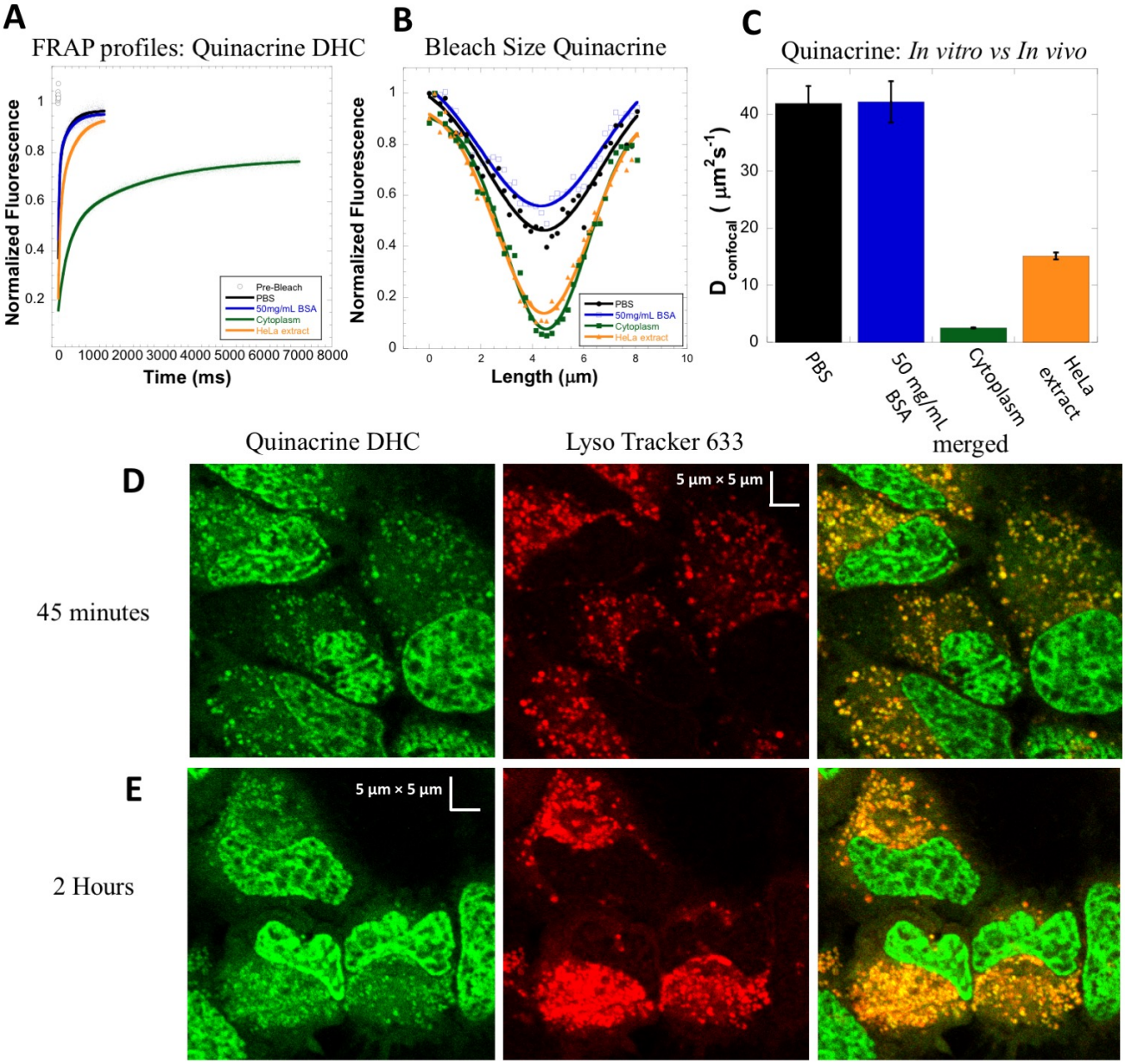

Figure 4. Diffusion of Quinacrine in PBS and in HeLa cells. Comparative (A) FRAP recovery profiles with exponential fits for Quinacrine dihydrochloride, (B) averaged bleach size profile with gaussian fits and (C) diffusion coefficients in PBS buffer, in 50mg/mL of BSA, HeLa cell extract and in live HeLa cells are shown. (D-E) Colocalization of Quinacrine DHC in lysosomal compartments are shown. HeLa cells were treated with Lyso Tracker 633 for 30 mins. Quinacrine DHC treatment was done for (D) 45 mins and (E) 2 hours respectively at 10 μM concentration.

Next, we compared FRAP of the cells treated with 2 and 6 μM quinacrine solutions after 2 and 24 h incubations (Figure S4A-F). The concentration of quinacrine had only a marginal effect on the results. Again, following 24 h incubation, very little quinacrine is free to diffuse in the cell.

Mitoxantrone, primaquine and amidoquine diffuse slowly in cells. For some drugs, like mitoxantrone (anti-cancer) and primaquine phosphate (antimalarial), we could not compare the diffusion coefficients *in*

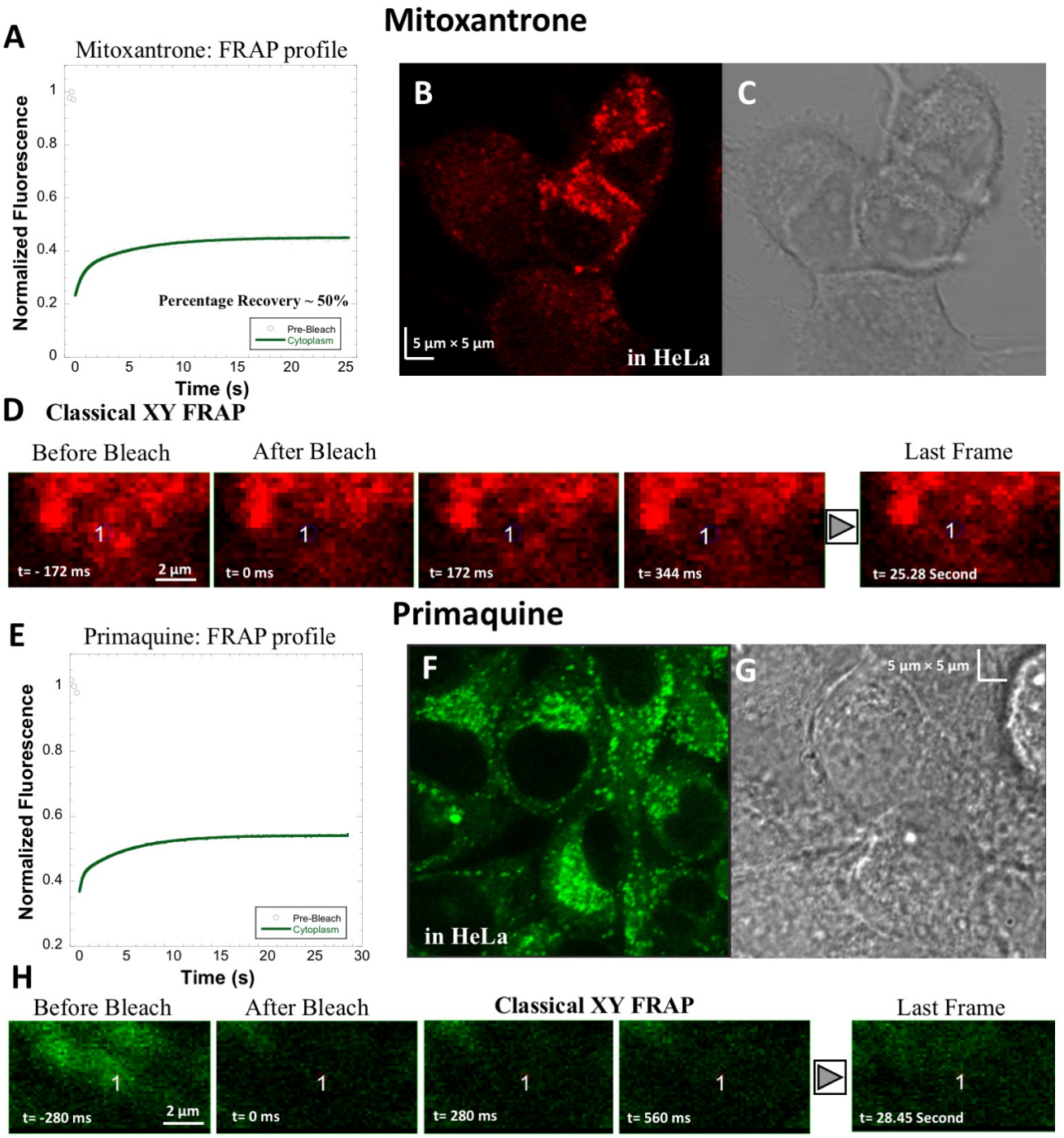

Figure 5. Mitoxantrone and Primaquine diffusion inside HeLa cells. XY- FRAP recovery profiles with exponential fits for (A) Mitoxantrone and (E) Primaquine in HeLa cells are shown. Fluorescent and Transmission channel images of HeLa cells after 45 mins incubations with (B-C) Mitoxantrone and (F-G) Primaquine are shown. Time lapse micrographs of a portion of HeLa cell going through a classical rectangular XY-FRAP protocol for (D) Mitoxatrone and, (H) Primaquine are also shown.

vitro and *in vivo*. The low quantum yields of these drugs and weak photo-stability prevented us from measuring their diffusion coefficients in buffer conditions using Line-FRAP. But, due to their slow diffusion, standard XY-FRAP could be used to obtain recovery rates (Figure 5A-H). Figures 5A and 5E show

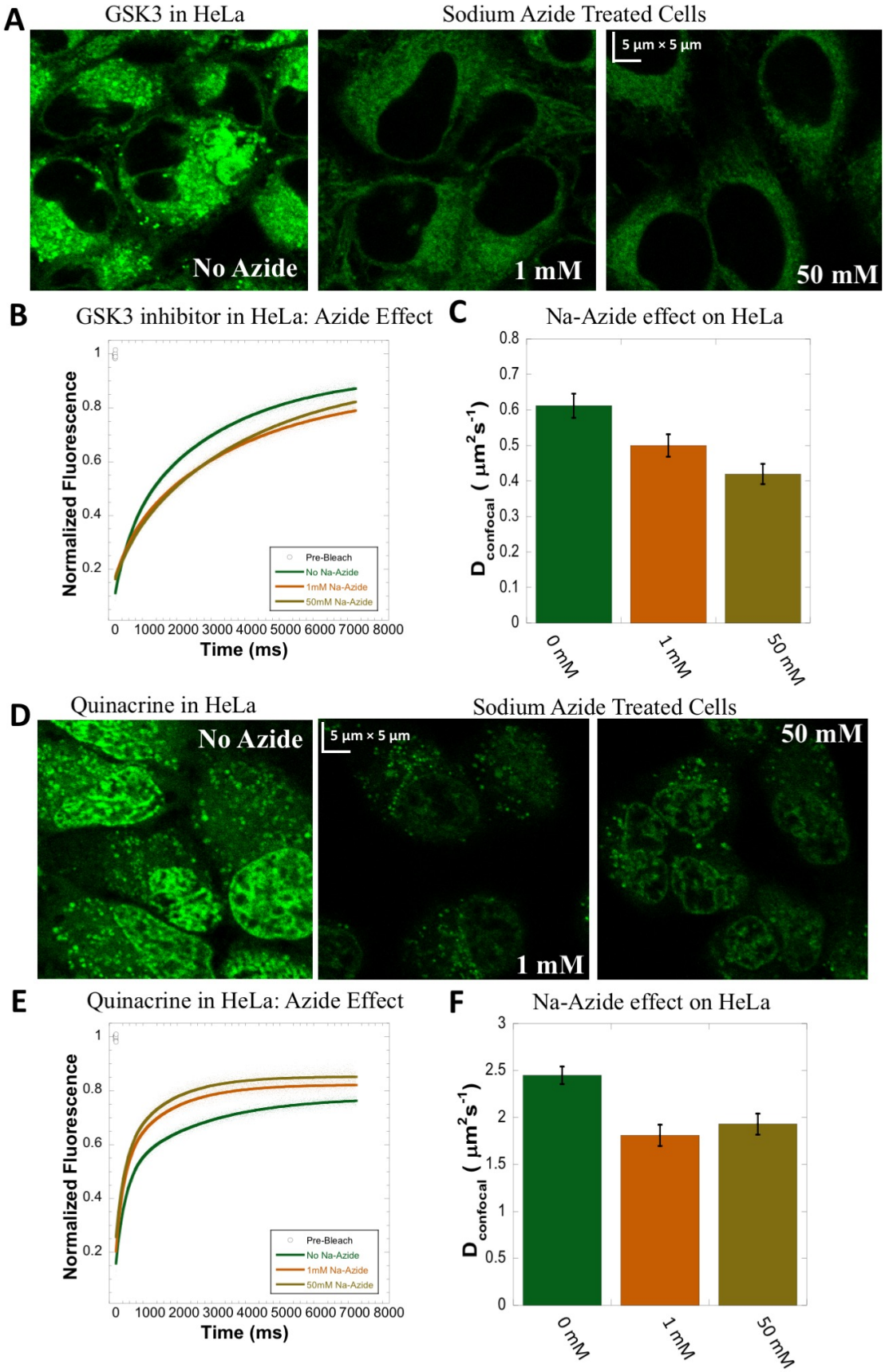

Figure 6. Effect of Na Azide on GSK3 inhibitor and Quinacrine diffusion inside the HeLa cells. (A) GSK3 inhibitor and (D) Quinacrine dihydrochloride treated HeLa cells with or without Na Azide treatment are shown. Comparison of FRAP profiles with exponential fits and calculated $D_{confocal}$ values for (B-C) GSK3 inhibitor and for (E-F) Quinacrine dihydrochloride are also shown.

that the percentage of recovery was very low, suggesting that these weakly basic drugs are also sequestered in the cellular cytoplasm. Confocal images in Figures 5B and 5F fully justify the FRAP recovery results. A colocalization study with LysoTracker red-633 suggests that Primaquine (S5A-B) and Amidoquine (S5C-D) are sequestered in lysosome chambers.

Lysosomal sequestration is not the key reason for slow diffusion of basic drugs in cells. Lysosomes an internal pH of ~4.5, maintained by vacuolar proton ATPase (V-H+-ATPase).[40,41] The non-protonated form of weakly basic small molecular drugs in the extracellular fluid enters the cytosol by simple diffusion. Depending on the p*K*a of the weak basic drugs, they become protonated in the acidic environment of the lysosome, becoming predominantly cationic, which hinders their back-diffusion to the cytosol. The phenomenon is known as cationic ion trapping[20,41] and results in drug accumulation in lysosomes up to millimolar concentrations.[40] To investigate whether lysosomal trapping is the main reason for the 20-40-fold lower diffusion in HeLa cells compared to the buffer-like conditions, we blocked lysosomal accumulation. For this we used Bafilomycin A1 or sodium azide prior to drug administration. Bafilomycin A1 is a specific V-ATPase inhibitor and stops the supply of protons in the lysosommal chamber.[37] As a result, cationic trapping can be considerably reduced. Figures S6A-B, and S7A-B show colocalization images for GSK3 inhibitor and quinacrine, respectively (with Lysotracker-633 used as marker) to follow the effect of 100 mM Bafilomycin A1 on drug accumulation.[42] The micrographs show that Bafilomycin strongly reduces quinacrine and GSK3 accumulation in the lysosomes (Figure S6A *vs* S6B and S7A *vs* S7B). Conversely, we do not see a large change in $D_{confocal}$ values after the treatment, which stay low. Comparative FRAP profiles and $D_{confocal}$ values are shown in Figures S6C-D and S7C-D for GSK3 inhibitor and Quinacrine, respectively. Calculated $D_{confocal}$ values remain almost unchanged, as shown in Figures S6D and S7D ($D_{confocal}$ for the GSK3 inhibitor is ~ 0.60 $\mu m^2 s^{-1}$, and for Quinacrine ~ 2.4 $\mu m^2 s^{-1}$). This suggests that Lysosomal accumulation of cationic drugs is contributing towards slower diffusion, but is not the key reason for the slow diffusion in the HeLa cell cytoplasm.

To verify the Bafilomycin results, HeLa cells were treated also with sodium azide, which inhibits vesicular structure growth in the cell cytoplasm.[39,43] Figure 6A and D show HeLa cells treated with 0, 1 and 50 mM sodium azide, followed by treatment with GSK3 inhibitor and quinacrine.[44] The micrographs in Figures 6B-C and 6E-F, show that sodium azide stopped lysosomal accumulation of these drugs. Comparative FRAP profiles and diffusion coefficients were not much changed for the two drugs and stayed low ($D_{confocal}$ are 1.4-1.9 $\mu m^2 s^{-1}$ for quinacrine and 0.42-0.61 $\mu m^2 s^{-1}$ for GSK3 inhibitor).

Exchanging the free amine groups with a carboxylic acid for three compounds highly increased their diffusion in the cell. The results so far show that some small molecules diffuse fast, while others diffuse very slowly within cells, which is often accompanied with low fraction recovery after FRAP. Moreover, the slow diffusion is not alleviated by inhibition of lysosomal sequestration. Strikingly, we found that slowly diffusing molecules in the cell are all weakly basic, compared to their anionic molecules, whose diffusion is not hindered (Figure S8). As over half of the small molecule drugs are basic,[6,7] this finding could have far reaching implications on drug efficiency. To prove this point, we compared diffusion of fluorescein disodium salt to that of 5-amino fluorescein (AM-Fluorescein, M.W.= 347.3 Da, Figure 7A), which is structurally similar but has an additional -NH_2 group and thus much higher p*K*a (Figure 7A). Figures 7B and D show FRAP traces for these molecules, and for CCF2. While fluorescein disodium salt has a fast FRAP rate, and is completely recovering, the cationic charged AM-fluorescein recovers much slower with a fraction recovery of 0.4. Moreover, while Fluorescein disodium salt is not sequestered in lysosomes, 5-Amino fluorescein is. As shown also for other compounds, adding sodium azide to the cells alleviates this sequestration (Figure 7C), but has only a small effect on the FRAP rate and fraction recovery (Figure 7D). Anionic CCF2, despite being larger than Fluorescein, recovers much faster than AM-fluorescein. This experiment strongly suggests that the functional primary amine group is the main contributor for the slow diffusion and low FRAP recovery inside the cell cytoplasm.

To further validate the role of basic amino groups in cell diffusion, we substituted the NH_2 of primaquine (antimalarial drug) and BODIPY compounds for the charge-neutral-NHAc functional group (Figure S9A and S10A). Due to their low quantum yield, we could not implement the faster Line-FRAP protocol, therefore, we used standard FRAP, which suits the slow diffusion of BODIPY. As seen from the FRAP profiles (time-dependent monographs) in Figure S9B-D for Primaquine derivatives and Figure S10B-C for BODIPY derivatives, the recovery is much slower for free amine-containing moieties. Figure S9I-J shows the percent recovery for unmodified primaquine is only at ~27%, whereas, for primaquine-NHAc, the recovery is ~60%. We have used both micro-injected and incubated cells for FRAP measurements for primaquine-NHAc, and the final results are the same. Unfortunately, the classical FRAP is not fast enough to calculate the diffusion coefficients, as the dead time was 150 ms. For the BODIPY analogues, the observations are similar, but to a smaller extend. For BODIPY-NH_2, the recovery percentage is ~57%, whereas, for BODIPY-NHAc, the recovery is ~67% (Figure S10H). The estimated recovery half-life also supports the observation, as shown in Figure S10I.

Competition between two drugs for lysosomal sequestration as a method for its inhibition. As previously discussed, anti-cancer drugs like mitoxantrone are designed to target the nucleus or cytosolic

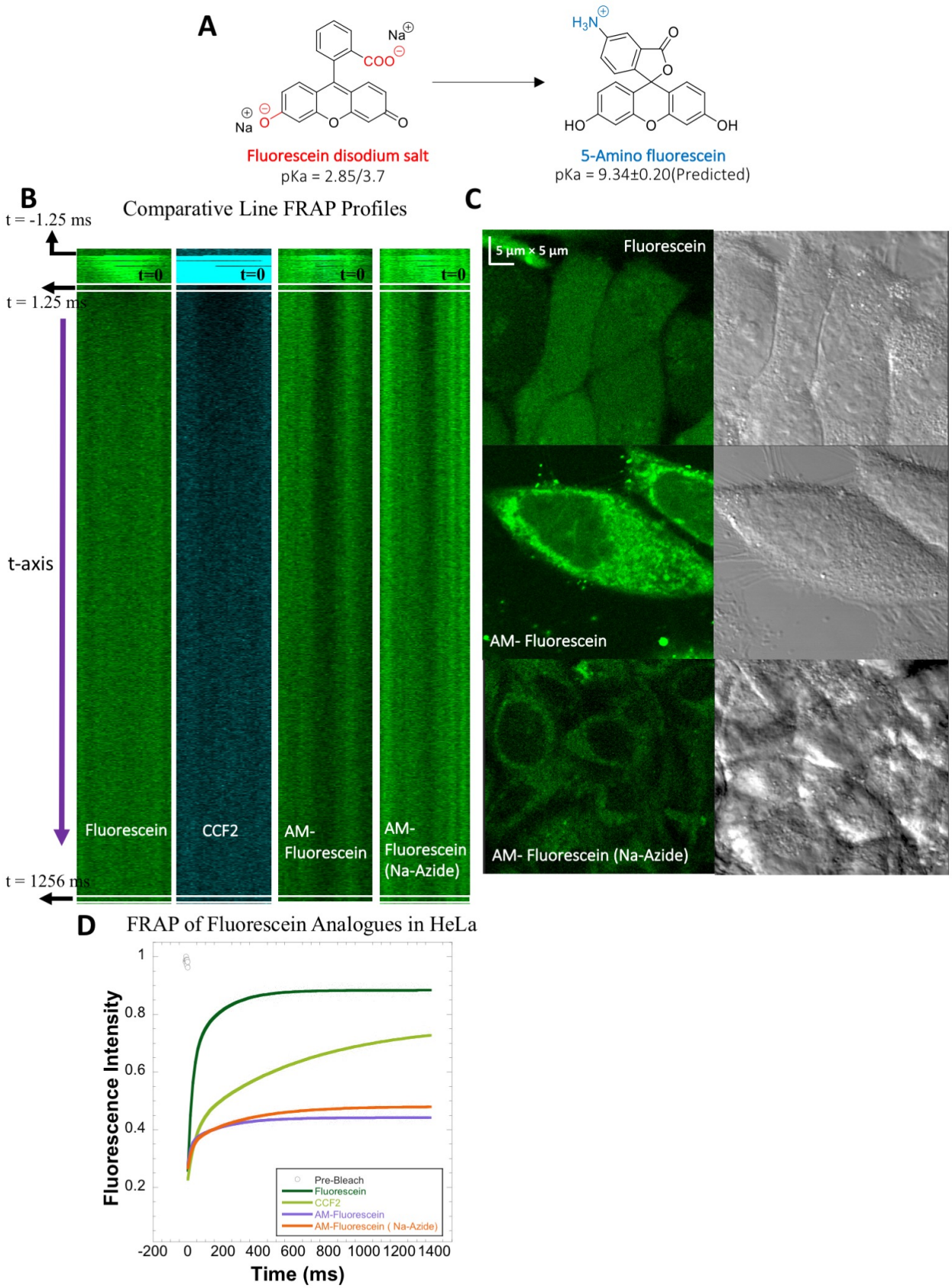

Figure 7. FRAP of Fluorescein analogues inside HeLa cells. (A) Structures of Fluorescein analogues with pKa values are shown. Comparative (B) Line FRAP profiles with time lapses, and (D) FRAP recoveries with exponential fits for Fluorescein, CCF2 and 5-amino Fluorescein, with/without Na-Azide treatments) in HeLa cells are shown. (C) Micrograph images of treated HeLa cells after drug incubations are also shown.

targets rather than lysosomes.[32] However, extensive sequestration reduces activity and promotes off-target

effects because of the lysosomotropic property. As shown in Figures 4 and 5, both quinacrine and mitoxantrone accumulate in the lysosome. Here, we investigated whether there is a preference for one or the other to be sequestrated. For this, we used different treatment sequences and drug doses[45] to shift drug localization properties. It is well known that lysosomes typically comprise less than 1% of total cell volume; however, the accumulation in lysosomes can account for most of a drug in the cell.[26] A competition between quinacrine and mitoxantrone drugs is shown in Figure 8. Treating first with mitoxantrone followed by quinacrine, resulted in mitoxantrone to accumulate in the lysosome and thus reducing its amount in the nucleus (Figure 8A). However, treating the cells first with quinacrine resulted in the mitoxantrone to reach the nucleus. quinacrine is the stronger basic drug compound between the two (pKa = 10.33 versus p*K*a = 9.08, respectively, as predicted by ChemAxon software[26]), resulting in its faster accumulation in the lysosomes. As a result, during the second treatment, mitoxantrone accumulated in the nucleus (Figure 8B), as seen also by staining the cells with Hoechst 33342 (Figure 8C). Calculating the colocalization coefficients provides a quantitative assessment of this phenomena (Figure 8D).

We wanted to ensure that this was not a spurious observation, therefore drug concentrations were varied (Figure S11). When quinacrine was first administered at 2 μM followed by mitoxantrone at 10 μM, the latter mostly accumulated in the lysosomes (Figure S11A). Increasing the dose of quinacrine to 4 and 10 μM (Figure S11 B-D) results in the lysosomes to be saturated with quinacrine, and as a result, mitoxantrone is accumulating in the nucleus. A similar observation was seen when reducing mitoxantrone to 4 μM Figure S12. It has been previously suggested that chloroquine and hydroxychloroquine enter the lysosomes and become protonated, which leads to their entrapment in acidic lysosomes and an increase in the lysosomal pH, which inhibits the lysosomal degradative enzymes.[46] This in turn, can lead, as shown above towards better targeting of anti-cancer drugs, such as mitoxantrone to the nucleus, with potential clinical benefits.

Proteins diffuse freely in the HeLa cytoplasm. To determine whether this phenomena of slow diffusion in the cell will be observed also for proteins, we determined the $D_{confocal}$ values and percent recovery as measured by FRAP for 15 different proteins (mostly from *E. coli*). These proteins were previously characterized by us to determine their oligomeric states in solution, with most of them being dimers or larger (Table S1 and [47]). All the proteins showed $D_{confocal}$ values of 18-28 $\mu m^2 s^{-1}$ in HeLa cell cytoplasm, typical for a cytoplasmic protein diffusion coefficient (Figure S13 A-B). Table S1 provides the predicted isoelectric points and net charge at pH 7.4 of the purified proteins as calculated by Prot Pi, showing all of them to be slightly acidic, as are the majority of *E.coli* cytosolic proteins.

DISCUSSION

In this study, we selected well-known and widely used small molecule drugs to study their behavior in aqueous solutions and living cells. All drug molecules used here are fluorescent, allowing for their FRAP measurements. Previously, we found that small-molecule drugs diffuse differently in crowded media than in a simple buffer solution, even if aggregation is not an issue.[13] Here, we show that many small molecules get trapped within the cellular cytoplasm, resulting in extremely slow diffusion and low fraction recovery after FRAP. This is particularly observed for cationic-charged small molecules, with $D_{confocal}$ values of 20-40-fold lower than observed for fluorescein or CF514. Even dense cell extract from HeLa cells is not mimicing the *in vivo* results (Figure 3A and C). This is very different from protein diffusion, where none of the 15 proteins measured here showed slow diffusion or low fraction recovery. Slow diffusion and low fraction recovery was limited to basic small molecules, showing $D_{confocal}$ values of 0.2-2 $\mu m^2 s^{-1}$. While the fraction recovery for all proteins is ~0.9, for many basic small molecules it is 0.2-0.5.

As primary culprit for the slow diffusion of the basic small molecule drugs, we suspected sequestration in the lysosomes. However, pre-treatment with sodium azide or Bafilomycin A1, which we showed to inhibit lysosomal accumulation, had only a small effect on diffusion or fraction recovery after FRAP, which stayed low. We also tested colocalization of GSK3 inhibitor in lipid droplets using the Nile red dye (Figure S14), in the ER using a specific BFP/mCherry tagged fluorescent antibody markers (Figure S15), and colocalization of Mitoxantrone with nucleic acids present in cytoplasm using SYTO blue (Figure S16). No colocalization was found between the drugs and either lipid droplets, the ER or nucleic acids. Super resolution images of GSK3 inhibitor treated HeLa cells were taken to improve the spatial distribution of it (Figure S17), however, this did not contribute new information to the puzzle. Therefore, we could not pinpoint the location of sequestration of weakly basic small molecule drugs within the cellular cytoplasm, except the lysosome.

The conclusive evidence that slow diffusion and low FRAP recovery results from the drugs being basic came by altering three molecules from being basic to acidic and vice versa. The best example here is fluorescein, which transformation to 5-amino fluorescein drastically reduced its diffusion as well as its fraction recovery after FRAP. Two additional examples here were Primaquine that was modified to Primaquine Acetate and BODIPY-NH_2 that was modified to BODIPY-NHAc. In both cases, the diffusion became faster and the fraction recovery increased significantly. This finding is important, as the activity of a drug within the cell is dictated by its active concentration. When the drug is sequestered, its active concentration is reduced. Even, if it is not fully sequestered, but only diffuses much slower, it will result

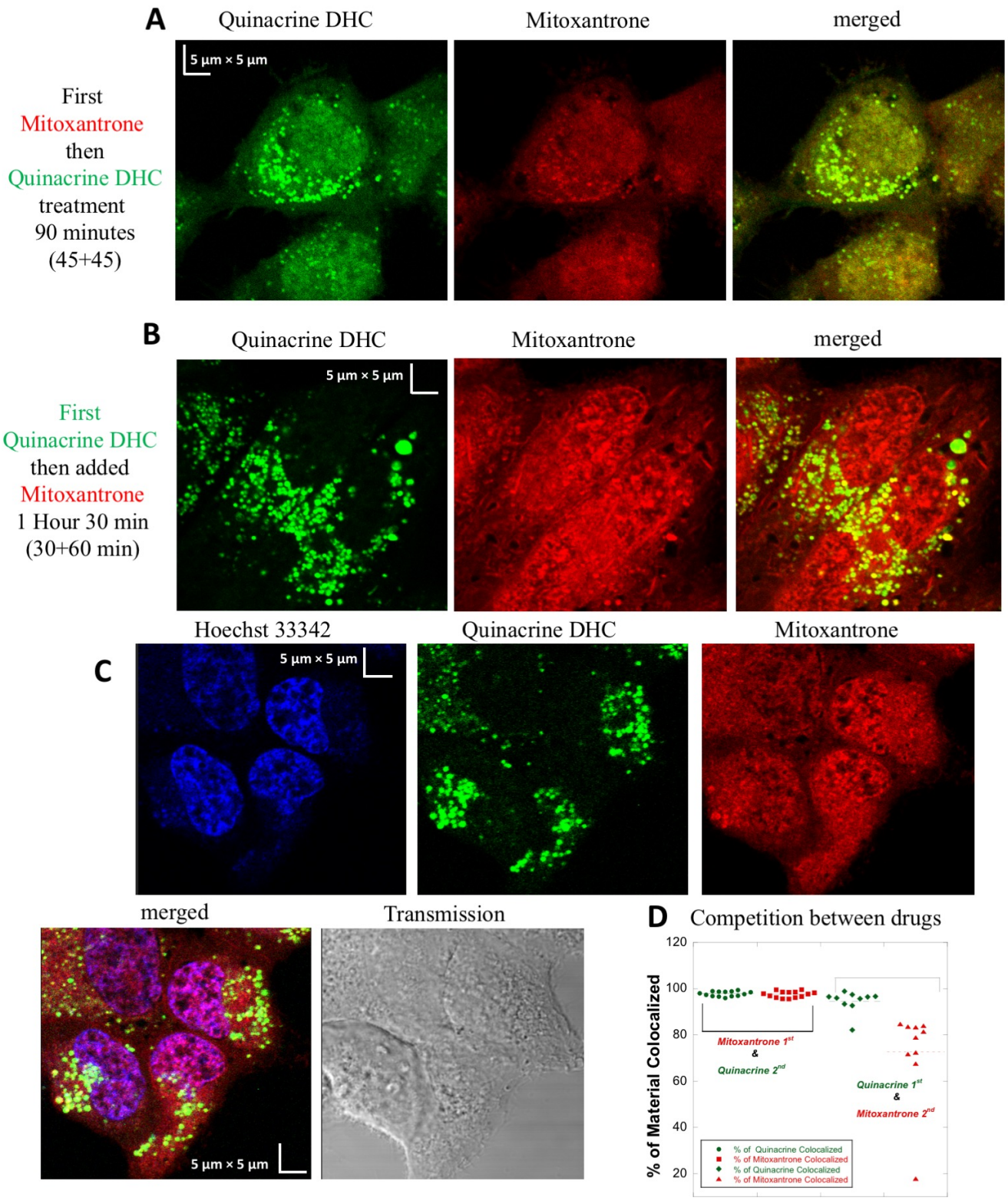

Figure 8: Colocalization of Mitoxantrone in lysosomal compartments. HeLa cells were (A) first treated with Mitoxantrone for 45 mins at 10 µM concentration, after which Quinacrine DHC was added and incubated for 45 mins. (B) First treatment with Quinacrine DHC for 30 mins, followed by Mitoxantrone treatment for 60 min is done . (C) Colocalization with hoechst 33342 dye for nuclear staining is also shown. (D) Quantitative assessment of Colocalization is also shown, each dot represents one micrograph containing multiple cell units (typically 3-5).

in slower association rate constant, and thus lower affinity towards the drug target (as most binding reac-

tions are diffusion limited). As a result, to keep the drug active, its dose has to be increased, which can have negative implications on side effects, due to off-target binding.

CONCLUSIONS

Our study shows that *in vitro* biophysical crowding studies for small molecule drugs are of limited value if one wants to understand the biophysical behavior of the same drug within the cell. While it is true that availability of a drug within a cell is only one factor dictating its biological activity, it is a crucial one. Our findings here raise an important limitation on the standard rules for drug design, as these do not consider the stickiness of basic small molecules within the cell. We were able to directly address this question by using fluorescent molecule drugs, and measuring their location and diffusion within cells. Most importantly, we also show that by blocking protonation of a number of basic compounds we were able to increase substantially their diffusion, and thus potentially their activity. These findings may be consequential in future drug development.

MATERIALS AND METHODS

All the reagents used are described in a table format (Table S2, Key resources). The supplementary method sections describe the synthetic procedures, characterizations, and purity of the synthesized compounds.

Mammalian Cell Culture. HeLa cells were grown in 35-mm glass-bottomed dishes (MatTek Corporation) in DMEM (1X) Gibco (Life Technologies Limited) supplemented with 1X pyruvate, penicillin/streptomycin (BioIndustries), and 10% fetal bovine serum (Life Technologies Limited). The cells were subcultured when 80% confluence was reached using trypsin-EDTA for cell detachment. $2x10^5$ HeLa cells in 2.5 ml of DMEM were pipetted into glass-bottomed dishes and incubated overnight. The cells were cultured in a humid atmosphere at 37 °C and 5% CO_2. The cells were imaged 24–30 h after seeding. Before the microinjection, the medium was aspirated, and fresh medium was supplemented with 25 mM HEPES, pH 7.4. For drug treatment, HeLa cells were incubated with 10 μM of drug (diluted 1:1000 from stock) for indicated times at 37 °C, followed by three times PBS 1X wash prior to imaging. For dose-dependent studies, the drug concentrations varied typically between 2-12 μM. Sodium azide concentration was 1 and 50 μM. Bafilomycin A1 was used at 100 nm concentration. Similarly, during the colocalization study, HeLa cells were treated with LysoTracker dye (1X) with 1:1000 dilution for 30 mins to 1 h at 37 °C, followed by 3x washing with PBS. Quinacrine, GSK3 inhibitor, Mitoxantrone, 5-amino Fluorescein, Amidoquine, Primaquine and BODIPY analogues were incubated with cells, while Fluorescein, Quinacrine, Primaquine-Ac, and CF514 dye were also micro-injected inside the HeLa cells.

Microinjection into HeLa cells. Microinjections were performed using the Eppendorf FemtoJet microinjector attached to the Eppendorf InjectMan NI2 micromanipulator. The fluorescein sodium salt, CCF2, CF514, quinacrine, primaquine analogues, BODIPY analogues were dissolved in DMSO and highly concentrated stock aliquots were made. A diluted PBS solution of small molecules were injected into cells using glass capillaries from Warner instruments and pulled by a vertical puller (Narishige). For every measurement, a single pressure pulse was applied to deliver the sample into the cell. Air was administrated at 15– 25 hPa for 0.1-0.3 s. For injections, single cells containing morphologically healthy and well-connected HeLa cells were selected. Before and after the microinjection, cell morphology and membrane integrity were confirmed by visually inspecting the injected cells.

HeLa cell extract preparation. Cytoplasmic HeLa cell extracts were prepared as described previously with slight modifications.[27] HeLa cells from 4×10 cm plates at 80% confluency were washed, treated with trypsin and collected. Pellets were mixed with 500µl of RIPA buffer, IMP40, 5 µL of protease inhibitor and stored in ice. After 20 min, the mixture was centrifuged at 13k×g. This process was repeated twice to obtain concentrated extract. A BSA calibration curve determined the total protein concentration; the final concentration was up to 100 mg/mL. After liquid nitrogen freezing, the final cell extract solution was stored at -80° C.

Protein purification and dye labeling. Bacterial proteins used in this study were purified as described by us previously. The dye labelling procedure with CF514 for purified proteins and removal of excess dye was described in detail.[28]

Confocal microscopy and FRAP Analysis. *Confocal microscopy.* Images were collected with an Olympus IX81 FluoView FV1000 Spectral/SIM Scanner confocal laser-scanning microscope, using 60X DIC oil-immersion objective, N.A. 1.35. For fluorescein sodium salt fluorescence measurements, excitation was done at 440 nm, using a diode laser at an output power of 1-4 % of maximal intensity for high to low concentrations. In contrast, emission was recorded from 520 to 550 nm using the spectral detection system. For CCF2-FA, excitation was done with the laser at 440 nm using 1-2 % of the maximal intensity, while emission was collected from 470-560 nm with SDM560 emission dichromator as cut-off filter. For quinacrine DHC and GSK3 inhibitor, excitation was done at 488 nm laser using 1-2% of the maximal intensity, while emission was collected from 502-560 nm with SDM560 emission dichromator as cut-off filter. During colocalization experiments of quinacrine DHC and GSK3 inhibitor with LysoTracker-633 dye, the same setting was used for detecting the small molecule drugs in Channel 1 (green). LysoTracker-633 dye was detected in Channel 2 (red) by exciting at 635 nm laser using 1-2 % of the maximal intensity, while emission was collected from 655-755 nm. For mitoxantrone and BODIPY analogues, excitation was done at 635 nm laser using 1-2 % of the maximal power, and emission was collected from 655-755

nm in Channel 2 (red). During the colocalization study of mitoxantrone in HeLa cells, quinacrine DHC served the Lysosome marker with the setting mentioned above for Channel 1 (green). Colocalization experiments with three colours were done for Hoechst-33342, quinacrine DHC, and mitoxantrone. The setup remains the same for quinacrine (green channel), mitoxantrone (red channel), with the addition of a 3rd channel (blue) for Hoechst dye. In the blue channel, excitation was done by 400 nm laser using 2-4% of maximal power, whereas the emission was collected from 420-480 nm with SDM480 emission dichromator as cut-off filter. The same setting is used in the blue channel for the SYTO blue maker (to visualize free nucleic acids) and blue fluorescent protein marker (BFP to visualize the ER). For the mcherry protein marker (to visualize the ER), the same setting for the red channel (Channel 2) is used. For every colocalization experiments, proper blank experiments were performed separately in all the respective channels with the same microscope settings to avoid any bleeding/leakage of emission signals from one Channel to another Channel, as shown in Figure S18. Image analyses were performed using FluoView/Imaris software, and data analyses were performed using Kaleidagraph software version 4.1 (Synergy). Colocalization coefficients as a percentage of material colocalized are calculated using Imaris software version 7.

Line-FRAP and Classical XY-FRAP. Line-FRAP was carried out in liquid drops and HeLa cells. For photobleaching, "Tornado" of 4 pixels (2x2) diameter.[28] It is the smallest area achievable using Tornado. The bleach circle was kept precisely in the middle of the scanning line. The lines we scanned were unidirectional with time intervals of 1.256 ms 1000 times (equivalent to 1.256 s) in the majority of the measurements. The number of scans prior to, during, and after the photobleaching was 10, 42, and 948, respectively. Only in some specific cellular measurements (for GSK3 inhibitor and Quinacrine DHC, where recovery is very slow) the unidirectional lines were scanned 5000 times. Photobleaching was achieved by using the laser at 405-nm or with 635-nm excitations for the 63-millisecond duration at full intensity (100%). The simultaneous scanner moved at a 100 µs/pixel speed to perform an efficient photo-bleach. We have used two simultaneous scanners during the Line-FRAP experiments: one scanner (at 405 nm with the full intensity of 100%) for photobleaching and another scanner (at 440/515/635 nm with weak intensity) for data acquisition.

For all the drugs except Mitoxantrone and BODIPY analogues (emission in red wavelengths), photobleach was performed by 405 nm laser. For fluorescence signal detection: fluorescein 440 nm laser (1-4%); CCF2 440 nm laser (1-2%); GSK3 inhibitor 440 nm laser (0-2%); quinacrine (1-2%) of maximal intensity were used. Emission collections were done from 520-550 nm for quinacrine DHC and GSK3 inhibitor.

Line FRAP was not possible for primaquine analogues, as it suffers from strong photo-bleach during recovery. Here classical XY FRAP was performed, with photo-bleach done by 405 nm laser with

full intensity. The frame rate is maintained at 172 ms with a bleach pulse duration was 150 ms. Due to microscope setting limitations, Line FRAP is also not feasible for Mitoxantrone and BODIPY analogues. A classical XY-FRAP using two simultaneous scanners is done for these molecules. Here, bleach was performed by simultaneous 635 nm laser with the full intensity of 100%, and the main excitation was done by 635 nm laser (with the power of 4%). Emission collections were done from 655-755 nm. For BODIPY analogues' FRAP recoveries, the bleach pulse time was 150 ms. The bleach pulse time was also 150 ms for primaquine analogues for comparative FRAP profile collections. The frame rate is maintained at 172 ms. Using the Olympus IX81 FluoView FV1000 Spectral/SIM Scanner confocal laser-scanning microscope, using Tornado (which requires SIM scanner to be loaded) greatly enhances bleaching efficiency. In addition, it shortens the time to obtain the first measurement after bleach (which is immediate in this mode). This property is highly beneficial for Line-FRAP measurements, where the time scale of data acquisition plays an important role. The Fluoview SIM scanner unit synchronizes laser light simulation with confocal and multiphoton imaging to avoid interruption to image observation during laser stimulation or manipulation. We have varied the intensity of the lasers to achieve an optimal signal/noise ratio. Fluorescence recovery plots were fitted to a double exponent growth curve. FRAP experiments were also performed inside the PBS buffer drops and crowding conditions. A coverslip was introduced at the top of the drop to stop evaporation during measurements. Our previously developed method on Line FRAP protocol has been employed to calculate diffusion coefficients from the FRAP rates and averaged bleach sizes. Diffusion rates cannot be calculated using XY-FRAP. However, FRAP parameters were kept constant so that qualitatively we could compare the average half-life and percentage of recoveries.

Determination of $D_{confocal}$ from FRAP results. We previously developed[28] the FRAP in Line mode (Line FRAP) method to monitor the diffusion rates of proteins in various environments. Line-FRAP allows a much faster data acquisition rate compared to classical XY FRAP. It is more suitable for measuring diffusion rates for fast diffusing molecules. The apparent diffusion coefficients calculated from Line FRAP measurements are $D_{confocal}$, which are calculated according to equation 1:

$$D_{confocal} = \frac{r_e^2 + r_n^2}{8\tau_{1/2}} \qquad \text{eq. 1}$$

where $t_{1/2}$ is the half-time of recovery and r_e and r_n is the effective and nominal bleach radii values (for details see [28]).

ASSOCIATED CONTENT

Supporting Information

The Supporting Information is available free of charge on the ACS Publications website.

brief description (file type, i.e., PDF)

brief description (file type, i.e., PDF)

AUTHOR INFORMATION

Corresponding Author

* Gideon Schreiber, Department of Biomolecular Sciences, Weizmann Institute of Science, Israel

AUTHORS

Debabrata Dey, Department of Biomolecular Sciences, Weizmann Institute of Science, Israel.

Shir Marciano, Department of Biomolecular Sciences, Weizmann Institute of Science, Israel**.**

Anna Poryvai, Institute of Organic Chemistry and Biochemistry of the Czech Academy of Sciences, Flemingovo náměstí 542/2, Prague 6, 160 00 Czech Republic

Ondrej Groborz, Institute of Organic Chemistry and Biochemistry of the Czech Academy of Sciences, Flemingovo náměstí 542/2, Prague 6, 160 00 Czech Republic

Lucie Wohlrábová, Institute of Organic Chemistry and Biochemistry of the Czech Academy of Sciences, Flemingovo náměstí 542/2, Prague 6, 160 00 Czech Republic

Tomás Slanina, Institute of Organic Chemistry and Biochemistry of the Czech Academy of Sciences, Flemingovo náměstí 542/2, Prague 6, 160 00 Czech Republic

Author Contributions

D.D. performed all the experiments. S.M. purified all the bacterial proteins. A.P, O.G., L.W., and T.S. designed the synthetic targets and synthesized primaquine acetate and BODIPY derivatives. D.D. and G.S. conceptualized the idea, analyzed the data and wrote the original draft of the manuscript. D.D., G.S., and T.S. reviewed and edited the paper. G.S. supervised the project. The manuscript was written through contributions of all authors. All authors have given approval to the final version of the manuscript.

Funding Sources

The Israel Science Foundation grant number 1268/18 (GS). The Czech Science Foundation (project No. 22-20319S) for funding this project (T.S.)

ACKNOWLEDGMENT

We would like to thank Dr. Ori Avinoam from Department of Biomolecular Sciences, and Prof. Hagen Hofmann from Department of chemical & structural Biology, Weizmann Institute of Science for their valuable discussions and advices. We want to acknowledge Dr. Reinat Nevo for her help with Imaris software to analyze the microscopy images.

ABBREVIATIONS

FRAP, fluorescence recovery after photo-bleaching; CCF2, coumarin cephalosporin fluorescein; BODIPY, boron dipyrromethene analogues; NMR, Nuclear magnetic resonance.

REFERENCES

1. Schreiber, S. L. Small Molecules: The Missing Link in The Central Dogma. *Nature Chemical Biology* **2005**, *1* (2), 64–66. https://doi.org/10.1038/nchembio0705-64.
2. Stockwell, B. R. Exploring Biology with Small Organic Molecules. *Nature* **2004**, *432*, 846–854. https://doi.org/10.1038/nature03196

3. Schreiber, S. L. The Small-Molecule Approach to Biology. Chemical genetics and diversity-oriented organic synthesis make possible the systematic exploration of biology. *Chemical & Engineering News* **2003**, *81* (9), 51–60. https://doi.org/10.1021/cen-v081n009.p051
4. Ngo, H. X.; Garneau-Tsodikova, S. What are the drugs of the future? *Med chem comm*. **2018**, *9* (5),757-758. https://doi.org/10.1039/C8MD90019A
5. Veber, D. F.; Johnson, S. R.; Cheng, Hung-Yuan; Smith, B. R.; Ward, K. W.; Kopple, K. D. Molecular Properties That Influence the Oral Bioavailability of Drug Candidates. *Journal of Medicinal Chemistry* **2002**, *45* (12), 2615-2623. https://doi.org/10.1021/jm020017n
6. Charifson, P. S.; Walters, W. P. Acidic and Basic Drugs in Medicinal Chemistry: A Perspective. *Journal of Medicinal Chemistry* **2014**, *57* (23), 9701-9717. https://doi.org/10.1021/jm501000a
7. Lipinski, C. A.; Lombardo, F.; Dominy, B. W.; Feeney, P. J. Experimental and Computational Approaches to Estimate Solubility and Permeability in Drug Discovery and Development Settings. *Advanced Drug Delivery Reviews* **1997**, *23* (1–3), 3–25. https://doi.org/10.1016/S0169-409X(96)00423-1
8. Manallack, D.T. The pK(a) Distribution of Drugs: Application to Drug Discovery. *Perspect Medicin Chem.* **2007**, *1*, 25–38. https://doi.org/10.1177/1177391X0700100003
9. Meanwell, N. A. Improving drug candidates by design: a focus on physicochemical properties as a means of improving compound disposition and safety. *Chem Res Toxicol.* **2011**, *24* (9), 1420-1456. https://doi.org/10.1021/tx200211v
10. Di, L.; Artursson, P.; Avdeef, A.; Ecker, G. F.; Faller, B.; Fischer, H.; Houston, J. B.; Kansy, M.; Kerns, E. H.; Krämer, S. D.; Lennernäs, H.; Sugano, K. Evidence-Based Approach to Assess Passive Diffusion and Carrier-Mediated Drug Transport. *Drug Discovery Today* **2012**, *17* (15–16), 905–912. https://doi.org/10.1016/j.drudis.2012.03.015.
11. Dobson, P. D.; Kell, D. B. Carrier-Mediated Cellular Uptake of Pharmaceutical Drugs: An Exception or the Rule? *Nature Reviews Drug Discovery* **2008**, *7* (3), 205–220. https://doi.org/10.1038/nrd2438.
12. Sugano, K.; Kansy, M.; Artursson, P.; Avdeef, A.; Bendels, S.; Di, L.; Ecker, G. F.; Faller, B.; Fischer, H.; Gerebtzoff, G.; Lennernaes, H.; Senner, F. Coexistence of Passive and Carrier-Mediated Processes in Drug Transport. *Nature Reviews Drug Discovery* **2010**, *9* (8), 597–614. https://doi.org/10.1038/nrd3187.
13. Dey, D.; Nunes-Alves, A.; Wade, R. C.; Schreiber, G. Diffusion of small molecule drugs is affected by surface interactions and crowder proteins. *iScience*, **2022**, *25* (10), 105088. https://doi.org/10.1016/j.isci.2022.105088
14. Model, M. A.; Hollembeak, J. E.; Kurokawa, M. Macromolecular crowding: A hidden link between cell volume and everything else. *Cellular Physiology and Biochemistry* **2021**, *55* (S1), 25-40. https://doi.org/10.33594/000000319
15. Fulton, A. B. How crowded is the cytoplasm? *Cell* **1982**, *30* (2), 345-347. https://doi.org/10.1016/0092-8674(82)90231-8
16. Ellis, R. J. Macromolecular crowding: Obvious but underappreciated. *Trends in Biochemical Sciences* **2001**, *26* (10), 597-604. https://doi.org/10.1016/S0968-0004(01)01938-7
17. Milo, R.; Phillips, R. Cell Biology by the Numbers. *Cell Biology by the Numbers*. **2015**, https://doi.org/10.1201/9780429258770
18. Neurohr, G. E.; Amon, A. Relevance and Regulation of Cell Density. *Trends in Cell Biology* **2020**, *30* (3), 213-225. https://doi.org/10.1016/j.tcb.2019.12.006
19. Madshus, I. H. Regulation of intracellular pH in eukaryotic cells. *The Biochemical journal* **1988**, *250* (1), 1–8. https://doi.org/10.1042/bj2500001

20. Asokan, A.; Cho, M. J. Exploitation of intracellular pH gradients in the cellular delivery of macromolecules. *Journal of Pharmaceutical Sciences* **2002**, *91* (4), 903-913. https://doi.org/10.1002/jps.10095
21. Proksch, E. pH in nature, humans and skin. *Journal of Dermatology* **2018**, *45* (9),1044-1052. https://doi.org/10.1111/1346-8138.14489
22. Long, X.; Zhang, X.; Chen, Q.; Liu, M.; Xiang, Y.; Yang, Y.; Xiao, Z.; Huang, J.; Wang, X.; Liu, C.; Nan, Y.; Huang, Q. Nucleus-Targeting Phototherapy Nanodrugs for High-Effective Anti-Cancer Treatment. *Frontiers in Pharmacology* **2022**, *13, 1-8*. Frontiers Media S.A. https://doi.org/10.3389/fphar.2022.905375
23. Tiwari, R.; Jain, P.; Asati, S.; Haider, T.; Soni, V.; Pandey, V. State-of-art based approaches for anticancer drug-targeting to nucleus. *Journal of Drug Delivery Science and Technology* **2018**, *48,* 383-392. https://doi.org/10.1016/j.jddst.2018.10.011
24. Jansen, G.; Barr, H.; Kathmann, I.; Bunni, M. A.; Priest, D. G.; Noordhuis, P.; Peters, G. J.; Assaraf, Y. G. Multiple mechanisms of resistance to polyglutamatable and lipophilic antifolates in mammalian cells: Role of increased folylpolyglutamylation, expanded folate pools, and intralysosomal drug sequestration. *Molecular Pharmacology*, **1999**, *55* (4),761-769. https://molpharm.aspetjournals.org/content/molpharm/55/4/761.full.pdf
25. Gotink, K. J.; Broxterman, H. J.; Labots, M.; de Haas, R. R.; Dekker, H.; Honeywell, R. J., Rudek, M. A.; Beerepoot, L. V.; Musters, R. J.; Jansen, G.; Griffioen, A. W.; Assaraf, Y. G.; Pili, R.; Peters, G. J.; Verheul, H. M. W. Lysosomal sequestration of sunitinib: A novel mechanism of drug resistance. *Clinical Cancer Research*, **2011**, *17* (23) 7337–7346. https://doi.org/10.1158/1078-0432.CCR-11-1667
26. Zhitomirsky, B., Assaraf, Y. G. Lysosomal sequestration of hydrophobic weak base chemotherapeutics triggers lysosomal biogenesis and lysosomedependent cancer multidrug resistance. *Oncotarget* **2015**, *6* (2), 1143-1156. https://doi.org/10.18632/oncotarget.2732
27. Zotter, A.; Bäuerle, F.; Dey, D.; Kiss, V.; Schreiber, G. Quantifying enzyme activity in living cells. *Journal of Biological Chemistry* **2017**, *292* (38), 15838–15848. https://doi.org/10.1074/jbc.M117.792119
28. Dey, D.; Marciano, S.; Nunes-Alves, A.; Kiss, V.; Wade, R. C.; Schreiber, G. Line-FRAP, A Versatile Method to Measure Diffusion Rates In Vitro and In Vivo. *Journal of Molecular Biology* **2021**, *433* (9), 166898. https://doi.org/10.1016/j.jmb.2021.166898
29. Ehsanian, R.; van Waes, C.; Feller, S. M. Beyond DNA binding - A review of the potential mechanisms mediating quinacrine's therapeutic activities in parasitic infections, inflammation, and cancers. *Cell Communication and Signaling* **2011**, *9* (13), 1-18. https://doi.org/10.1186/1478-811X-9-13
30. Camarda, G.; Jirawatcharadech, P.; Priestley, R. S.; Saif, A.; March, S.; Wong, M. H. L.; Leung, S.; Miller, A. B.; Baker, D. A.; Alano, P.; Paine, M. J. I.; Bhatia, S. N.; O'Neill, P. M., Ward, S. A., Biagini, G. A. Antimalarial activity of primaquine operates via a two-step biochemical relay. *Nature Communications* **2019**, *10* (1), 3226, 1-9. https://doi.org/10.1038/s41467-019-11239-0
31. Olliaro, P.; Mussano, P. (2009). Amodiaquine for treating malaria. *Cochrane Database of Systematic Reviews* **2003**, *2*, CD000016, 1-69. https://doi.org/10.1002/14651858.CD000016
32. Shenkenberg, T. D.; von Hoff, D. D. Mitoxantrone: A new anticancer drug with significant clinical activity. *Annals of Internal Medicine* **1986**, *105*, 1, 67-81. https://doi.org/10.7326/0003-4819-105-1-67
33. Wagman, A.; Johnson, K.; Bussiere, D. Discovery and Development of GSK3 Inhibitors for the Treatment of Type 2 Diabetes. *Current Pharmaceutical Design* **2005**, *10* (10), 1105–1137. https://doi.org/10.2174/1381612043452668

34. Jampol, L. M.; Cunha-Vaz, J. *Diagnostic Agents in Ophthalmology: Sodium Fluorescein and Other Dyes* **1984**, *69*, 699–714. https://doi.org/10.1007/978-3-642-69222-2_21
35. Zuverink, M.; Barbieri, J. T. From GFP to β-lactamase: advancing intact cell imaging for toxins and effectors. *Pathogens and Disease* **2015** *73* (9), 699–714. https://doi.org/10.1093/femspd/ftv097
36. Poryvai, A.; Galkin, M., Shvadchak, V., Slanina, T. Red-Shifted Water-Soluble BODIPY Photocages for Visualisation and Controllable Cellular Delivery of Signaling Lipids. *Angew. Chemie - Int. Ed.* **2022**, *61* (34), e202205855. https://doi.org/10.1002/anie.202205855
37. Wang, R.; Wang, J.; Hassan, A.; Lee, C. H.; Xie, X. S.; Li, X. Molecular basis of V-ATPase inhibition by bafilomycin A1. *Nature Communications* **2021**, *12* (1),1782, 1-8. https://doi.org/10.1038/s41467-021-22111-5
38. Spugnini, E. P.; Citro, G.; Fais, S. Proton pump inhibitors as anti vacuolar-ATPases drugs: A novel anticancer strategy. *Journal of Experimental and Clinical Cancer Research* **2010**, *29* (1), 44. https://doi.org/10.1186/1756-9966-29-44
39. Hiruma, H.; Katakura, T.; Takenami, T.; Igawa, S.; Kanoh, M.; Fujimura, T.; Kawakami, T. Vesicle disruption, plasma membrane bleb formation, and acute cell death caused by illumination with blue light in acridine orange-loaded malignant melanoma cells. *Journal of Photochemistry and Photobiology B: Biology* **2007**, *86* (1), 1-8. https://doi.org/10.1016/j.jphotobiol.2006.08.003
40. de Duve, C.; de Barsy, T.; Poole, B.; Trouet, A; Tulkens, P.; van Hoof, F. Commentary. Lysosomotropic agents. *Biochemical Pharmacology* **1974**, *23* (18), 2495-2531. https://doi.org/10.1016/0006-2952(74)90174-9
41. Kaufmann, A. M.; Krise, J. P. Lysosomal sequestration of amine-containing drugs: Analysis and therapeutic implications. *Journal of Pharmaceutical Sciences* **2007**, *96* (4), 729-746. https://doi.org/10.1002/jps.20792
42. Yoshimori, T.; Yamamoto, A.; Moriyama, Y.; Futai, M.; Tashiro, Y. Bafilomycin A1, a specific inhibitor of vacuolar-type H+-ATPase, inhibits acidification and protein degradation in lysosomes of cultured cells. *Journal of Biological Chemistry* **1991,** *266* (26),17707-17712. https://doi.org/10.1016/s0021-9258(19)47429-2
43. Ishii, H.; Shirai, T.; Makino, C.; Nishikata, T. Mitochondrial inhibitor sodium azide inhibits the reorganization of mitochondria-rich cytoplasm and the establishment of the anteroposterior axis in ascidian embryo. *Development Growth and Differentiation* **2014**, *56* (2), 175-188. https://doi.org/10.1111/dgd.12117
44. Poste, G.; Papahadjopoulos, D. Lipid vesicles as carriers for introducing materials into cultured cells: influence of vesicle lipid composition on mechanism(s) of vesicle incorporation into cells. *Proceedings of the National Academy of Sciences of the United States of America* **1976**, *73* (5), 1603-1607. https://doi.org/10.1073/pnas.73.5.1603
45. Guieu, B., Jourdan, J. P., Dreneau, A., Willand, N., Rochais, C., & Dallemagne, P. Desirable drug–drug interactions or when a matter of concern becomes a renewed therapeutic strategy. *Drug Discovery Today* **2021**, *26* (2), 315-328. https://doi.org/10.1016/j.drudis.2020.11.026
46. Verbaanderd, C.; Maes, H.; Schaaf, M. B.; Sukhatme, V. P.; Pantziarka, P.; Sukhatme, V.; Agostinis, P.; Bouche, G. Repurposing drugs in oncology (ReDO) - Chloroquine and hydroxychloroquine as anti-cancer agents. *Ecancermedicalscience* **2017**, *11,*781, 1-35. https://doi.org/10.3332/ecancer.2017.781
47. Marciano, S.; Dey, D.; Listov, D.; Fleishman, S.J.; Sonn-Segev, A.; Mertens, H.; Busch, F.; Kim, Y.; Harvey, S.R.; Wysocki, V.H.; Schreiber, G. Protein quaternary structures in solution are a mixture of multiple forms. *Chem Sci.* **2022**, *13* (39), 11680-11695. https://doi.org/10.1039/d2sc02794a

Insert Table of Contents artwork here

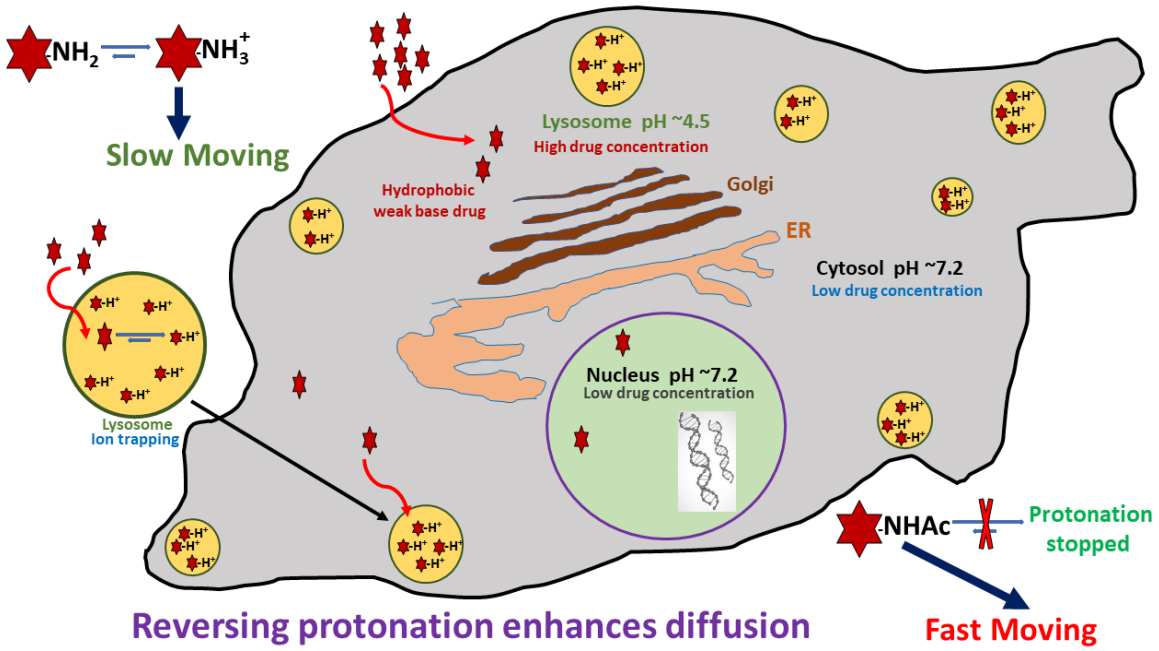

Supplementary Figure S1-S26

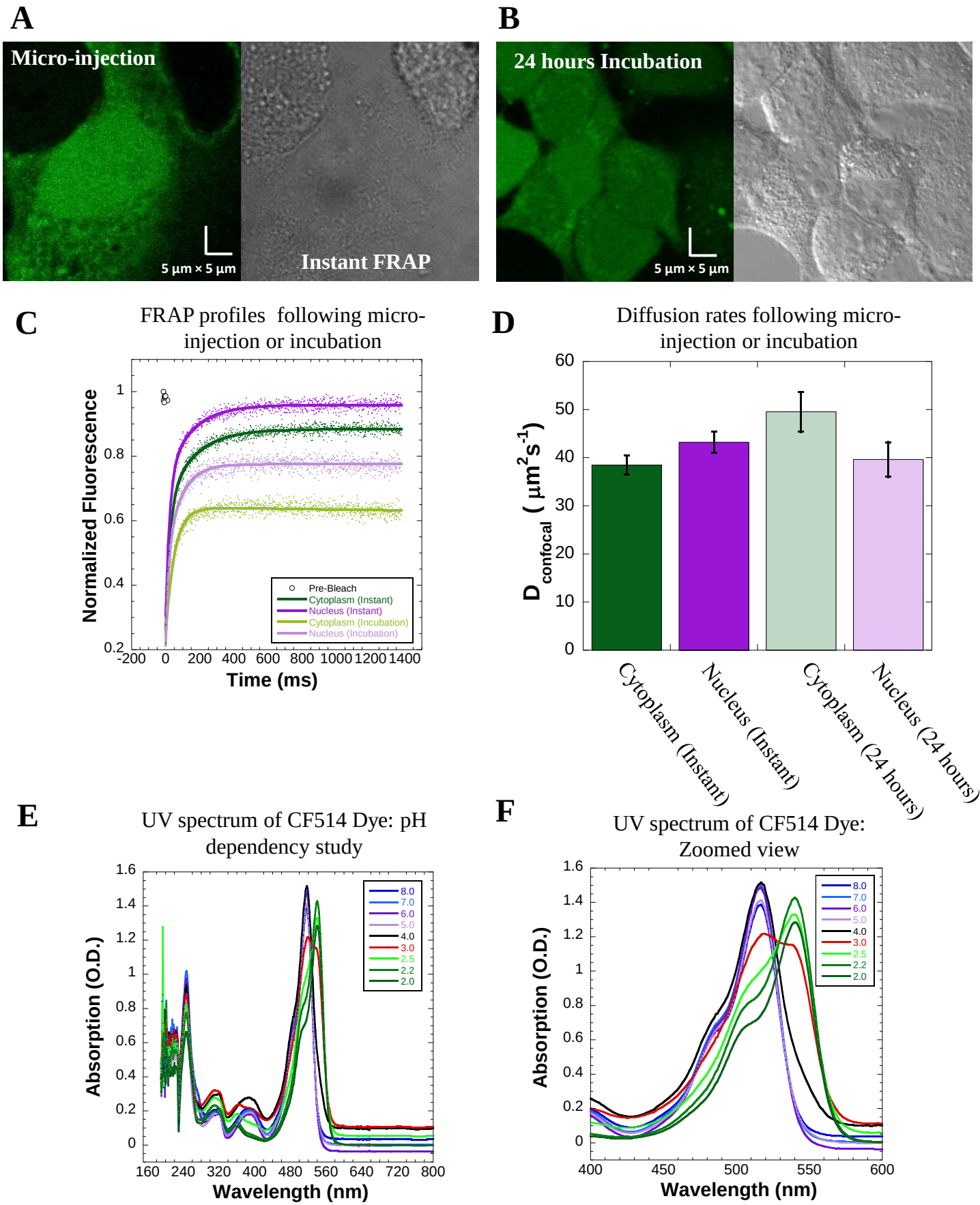

Figure S1: FRAP measurements for Fluorescein following different incubation times. Micrographs of HeLa cells (A) instantaneously after micro-injection *vs* (B) FRAP after 24 hours incubation are shown. Comparative (C) FRAP profiles with fits and (D) $D_{confocal}$ values are also shown. (E-F) Comparative UV spectrum of CF514 labelling dye in 20 mM sodium phosphate buffer at different pH values are shown, which predicts CF514 dye p*K*a~ 3.

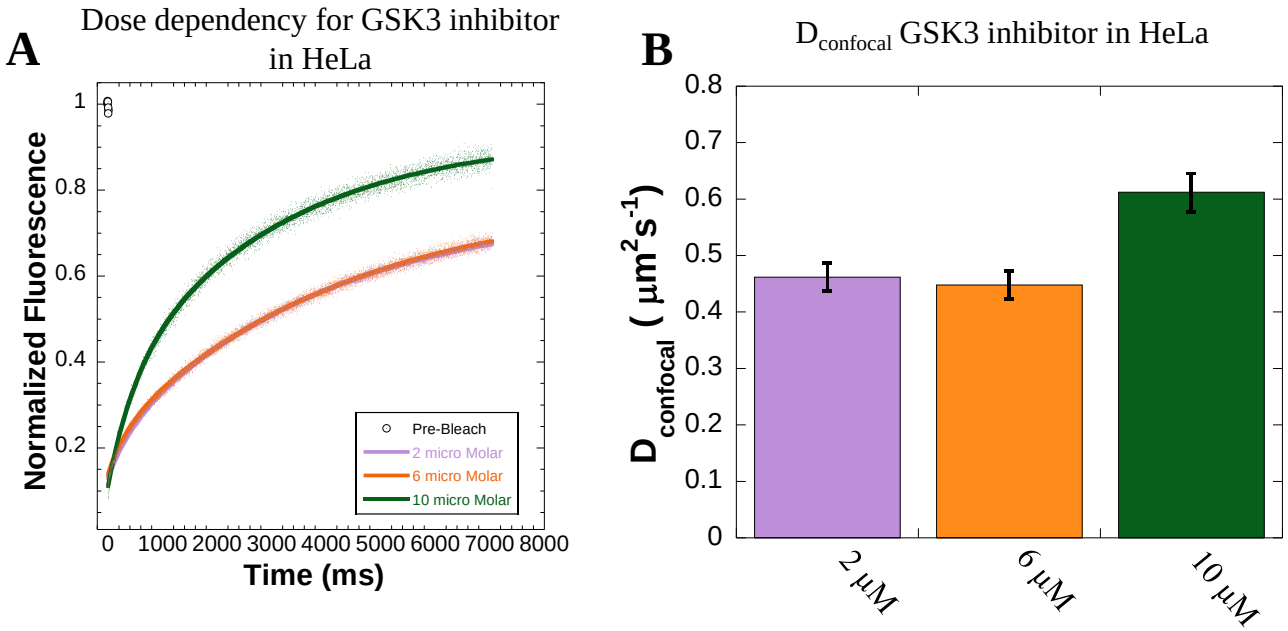

Figure S2: Diffusion rates and dose dependency of GSK3 inhibitor inside HeLa.(A-B) Drug dose dependency of GSK3 inhibitor treated HeLa cells. Effect of drug dosage (2-10 μM) on (A) FRAP profiles with fits and (B) diffusion coefficients are also shown.

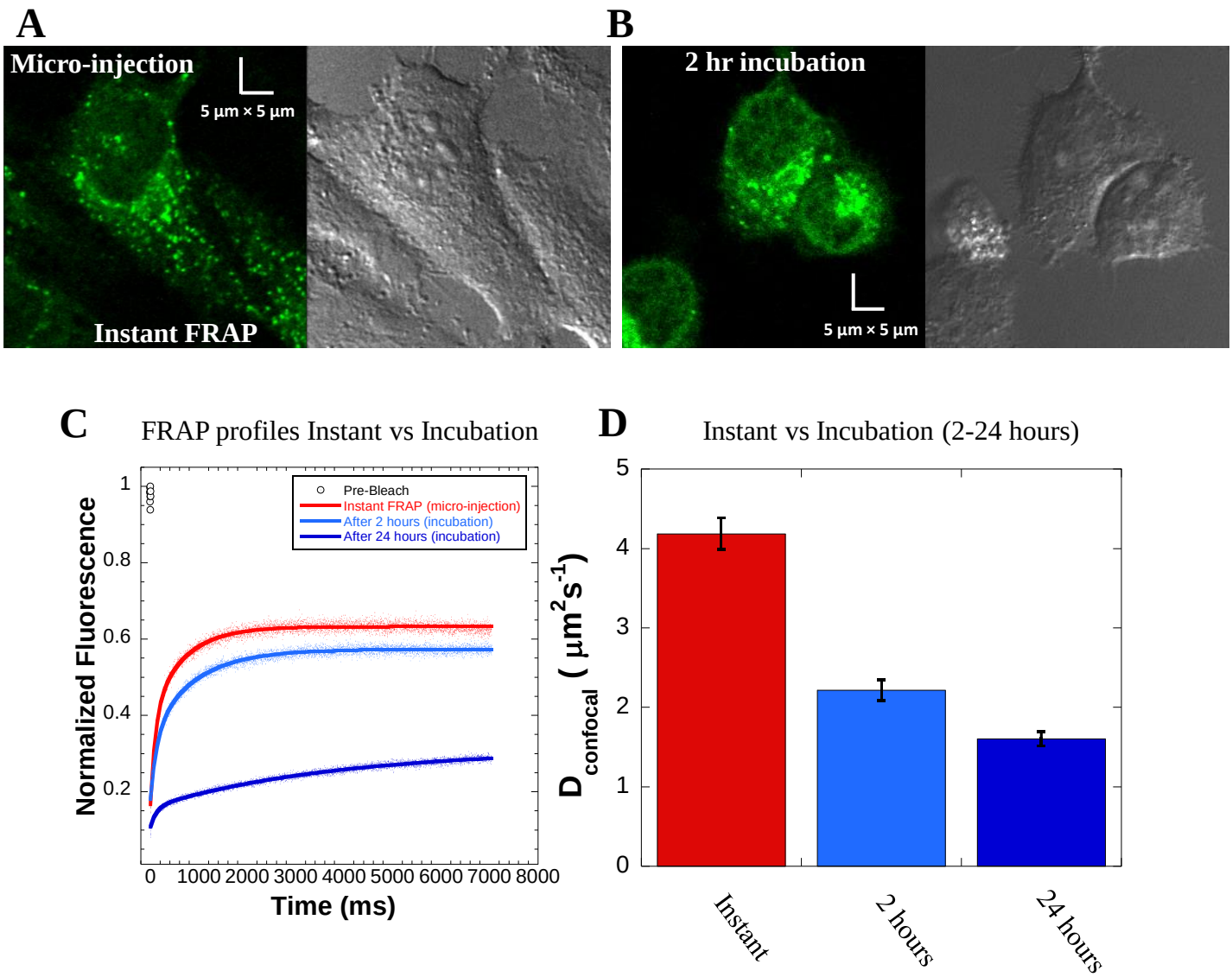

Figure S3: Quinacrine diffusion upon micro-injection or after incubation. Comparison of FRAP instantaneously following micro-injection (instant FRAP) and FRAP following 2-24 hr incubation are shown. HeLa cell micrographs following (A) micro-injection and (B) 2 hours of incubation are shown. Comparative (C) FRAP profiles with exponential curve fits and (D) calculated $D_{confocal}$ values are also shown.

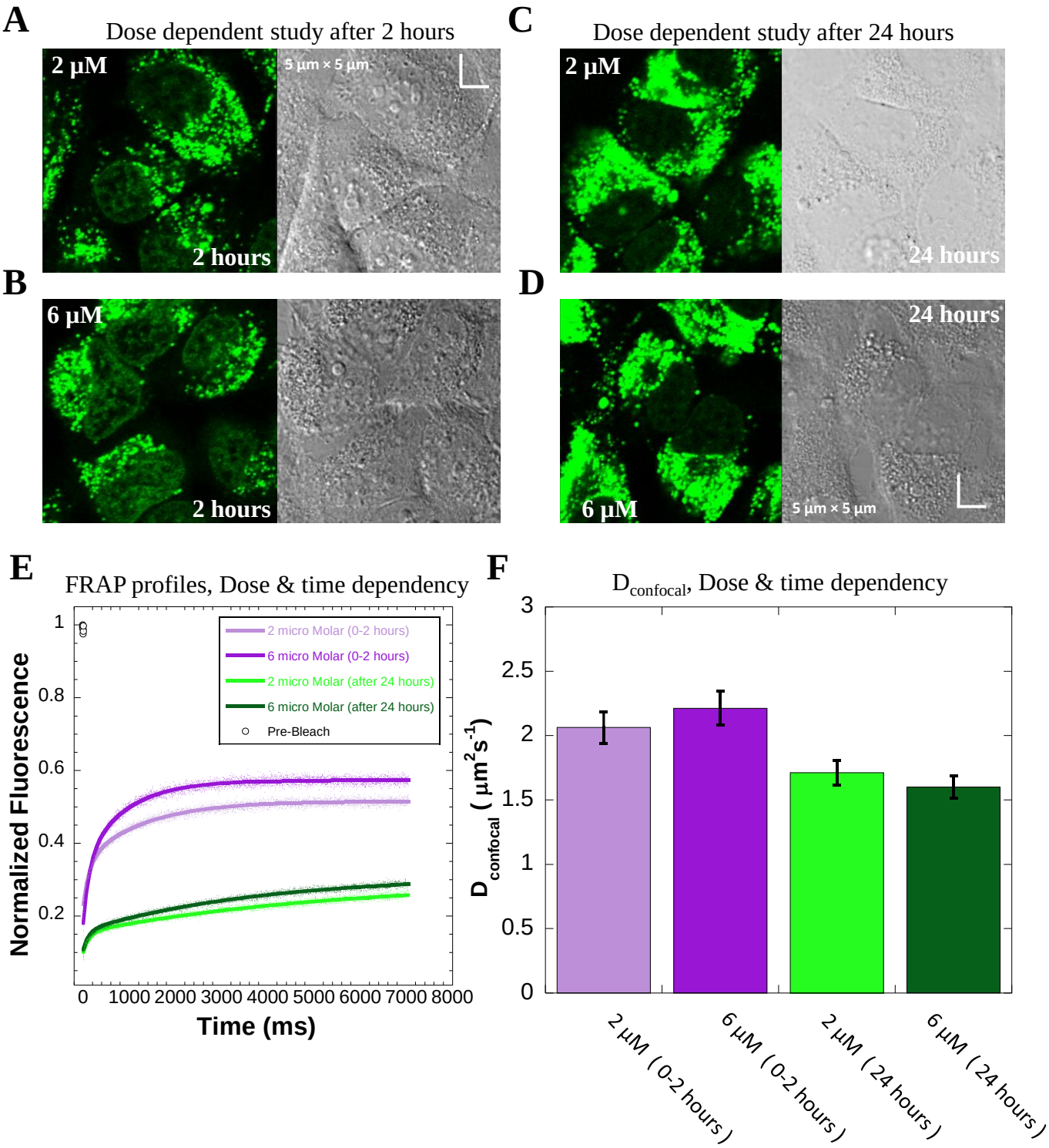

Figure S4: Dose and time dependency of Quinacrine inside HeLa. HeLa cell micrographs s after 2 hours of incubation with (A) 2 µM and (B) 6 µM of Quinacrine dose are shown. (C) and (D) are micrographs of HeLa cells after 24 hours of treatment with Quinacrine at 2 µM and 6 µM respectively. Effect of drug dose and time dependency on comparative (E) FRAP profiles with fits, and (F) calculated $D_{confocal}$ values are also shown .

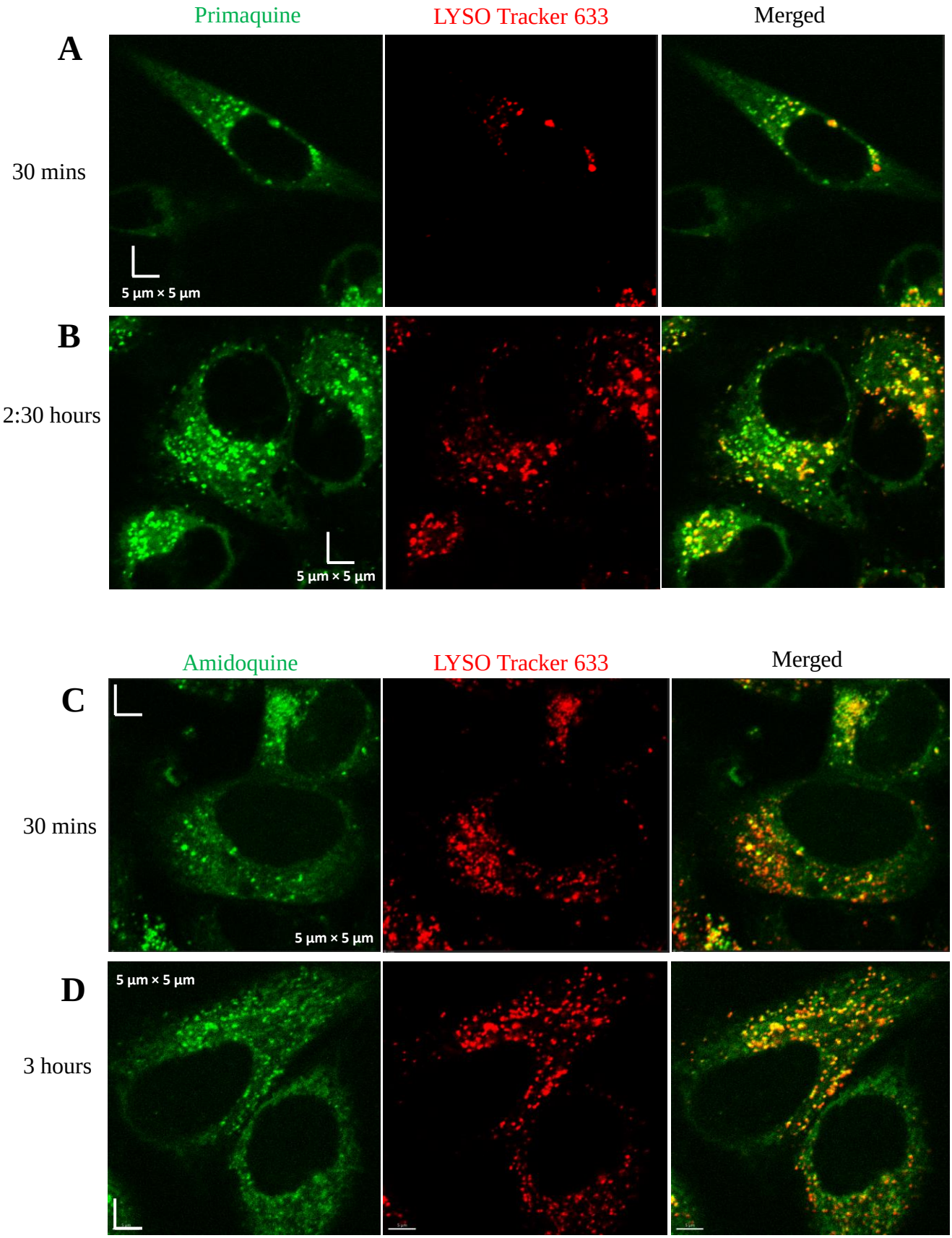

Figure S5: Colocalization of Primaquine and Amidoqiuine to Lyso-tracker. Colocalization of Primaquine (A-B) and Amidoquine (C-D) drugs with Lyso Tracker 633 in HeLa cells are shown. Time dependent measurements show higher aggregation of both drugs in the lysosomes of the cells over time.

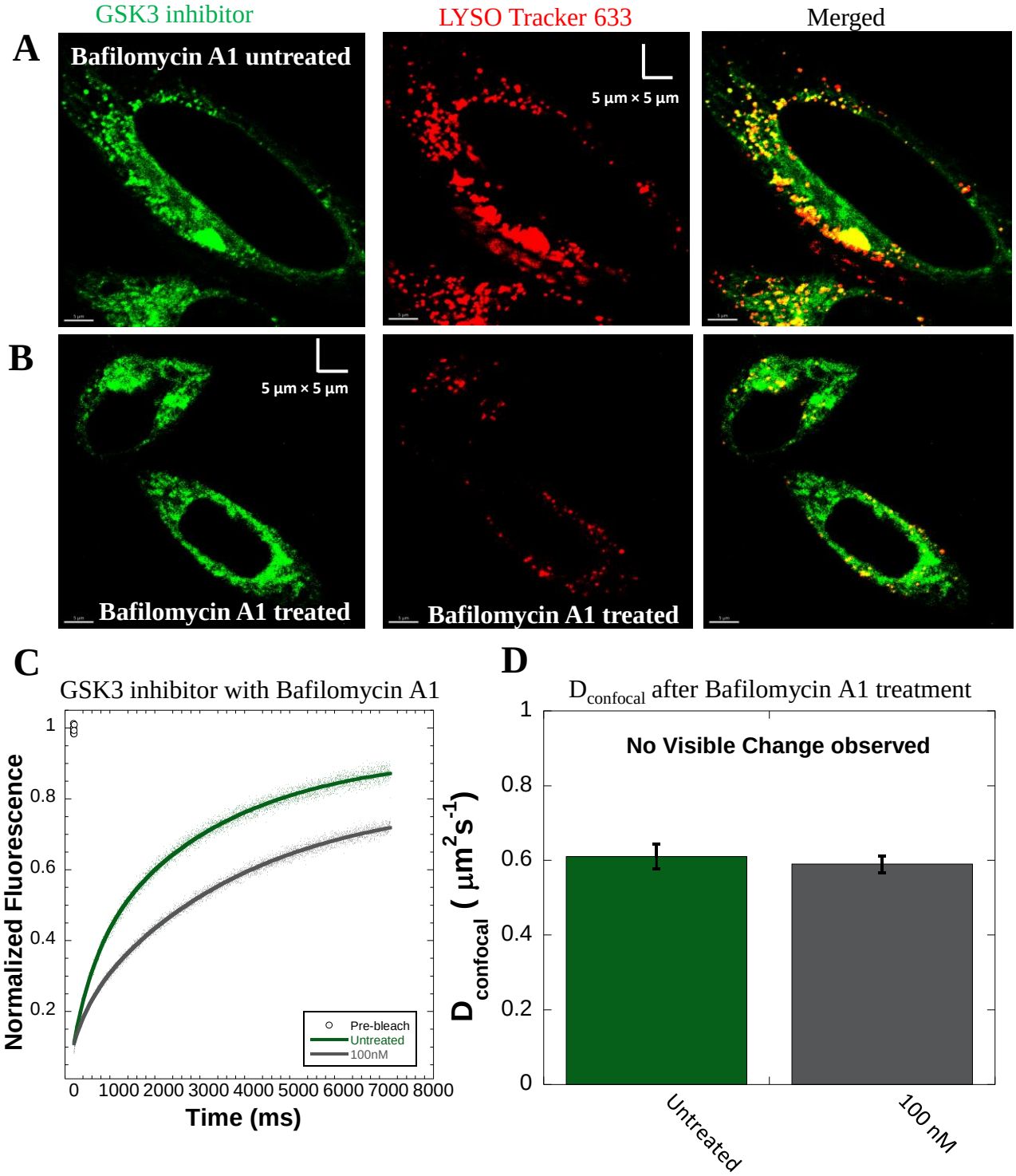

Figure S6: Inhibiting lysosomal accumulation of GSK3 inhibitor using. (A-B) Colocalization of GSK3 inhibitor with Lyso Tracker 633 in HeLa cells are shown. HeLa cells (A) untreated and (B) treated with 100 nM Bafilomycin A1 and corresponding colocalizations are shown. Comparative (C) FRAP profiles with fits and (D) $D_{confocal}$ values with and without the Bafilomycin A1 treatment are also shown.

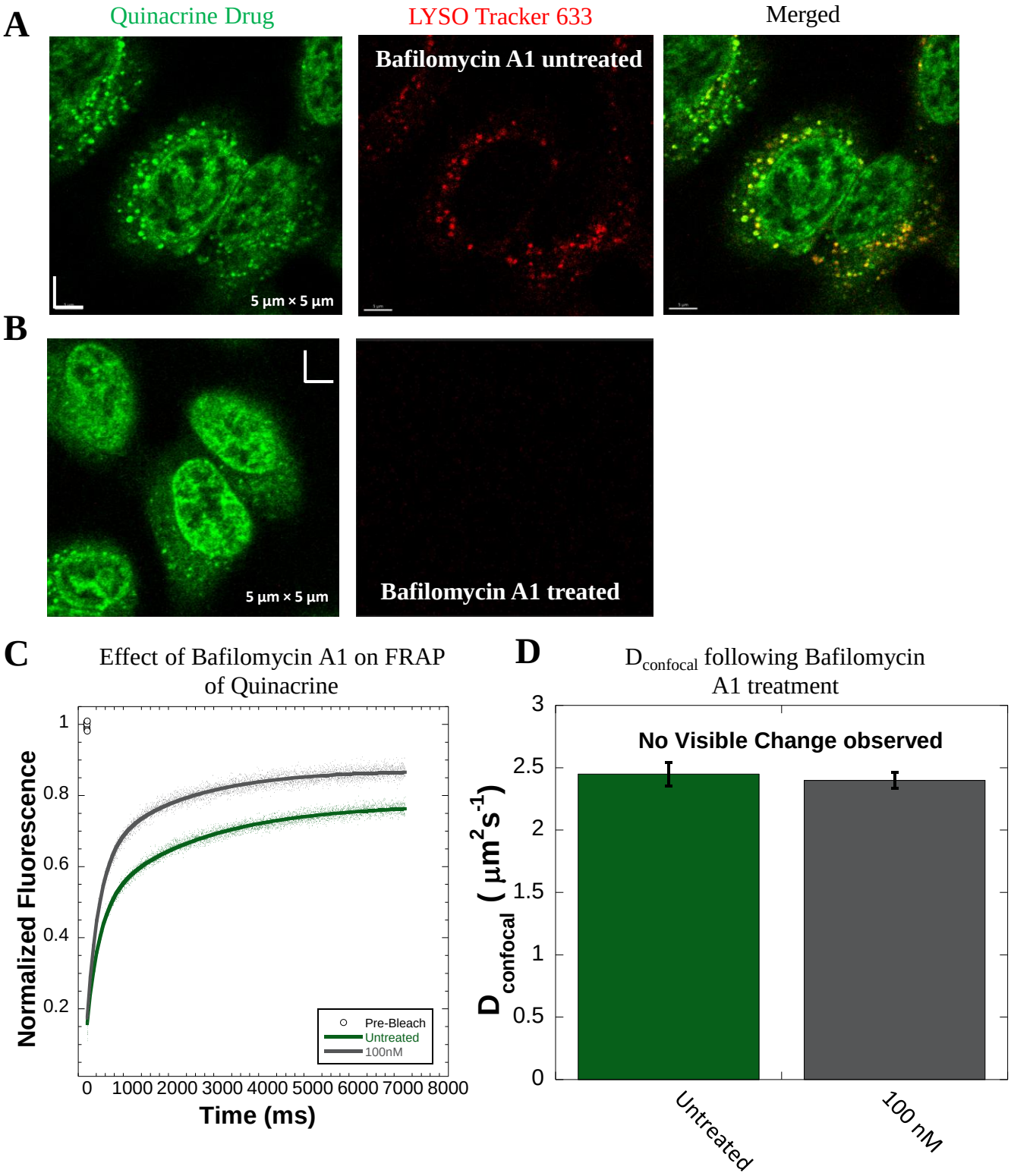

Figure S7: Bafilomycin A1 effect on diffusion of Quinacrine in HeLa cells. (A-B) Colocalization of Quinacrine with Lyso Tracker 633 in HeLa cells are shown. HeLa cells (A) untreated and (B) treated with 100 nM Bafilomycin A1 and corresponding colocalizations are shown. Comparative (C) FRAP profiles with fits and (D) $D_{confocal}$ values with and without the Bafilomycin A1 treatment are also shown.

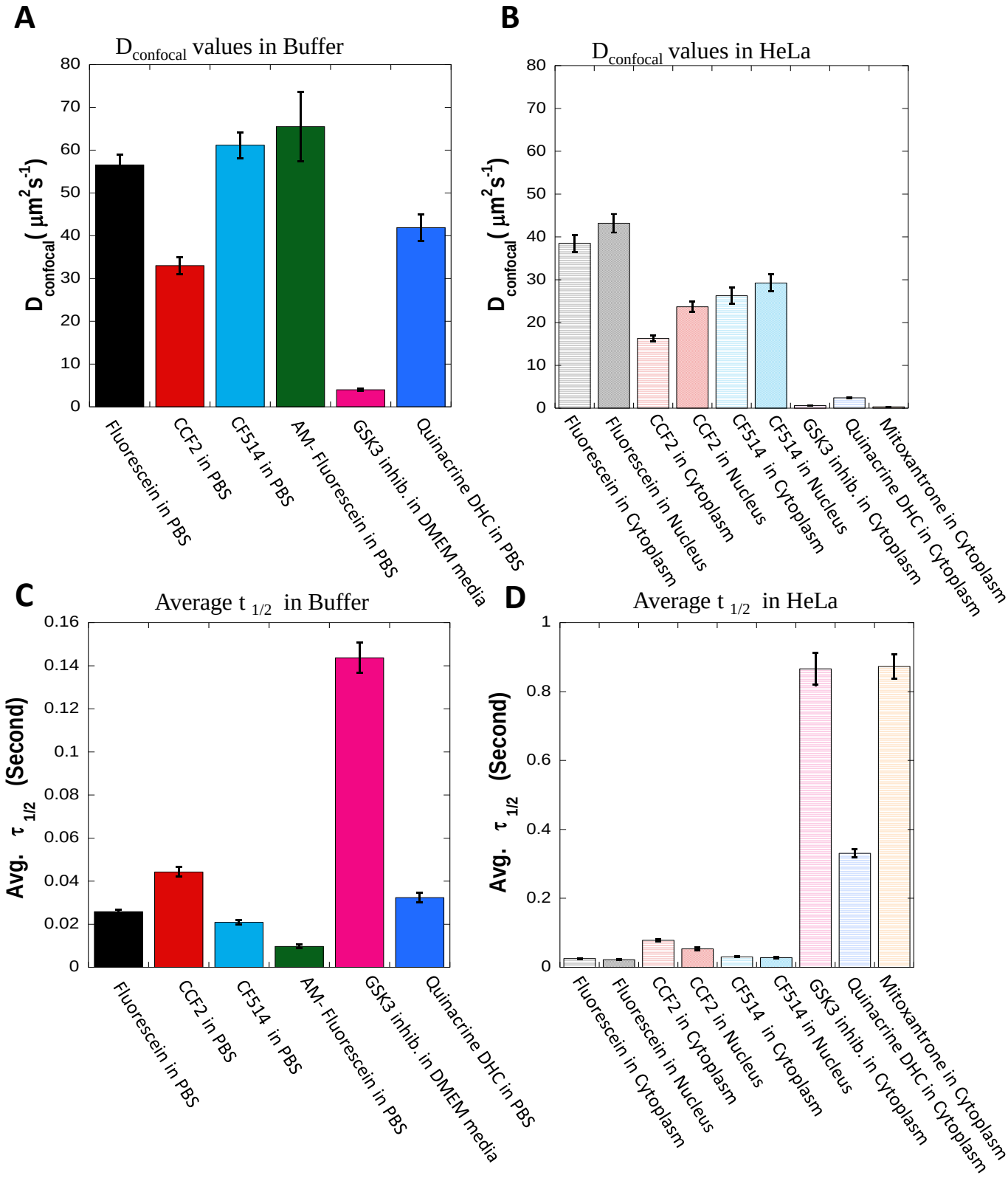

Figure S8: Diffusion coefficients of small molecules in PBS buffer and inside HeLa cells. Comparison of $D_{confocal}$ values of small molecule drugs in (A) PBS buffer and in (B) HeLa cells are shown. Comparison of average half-times $t_{1/2}$ of small molecule drugs in (C) PBS buffer and in (D) HeLa cells are also shown.

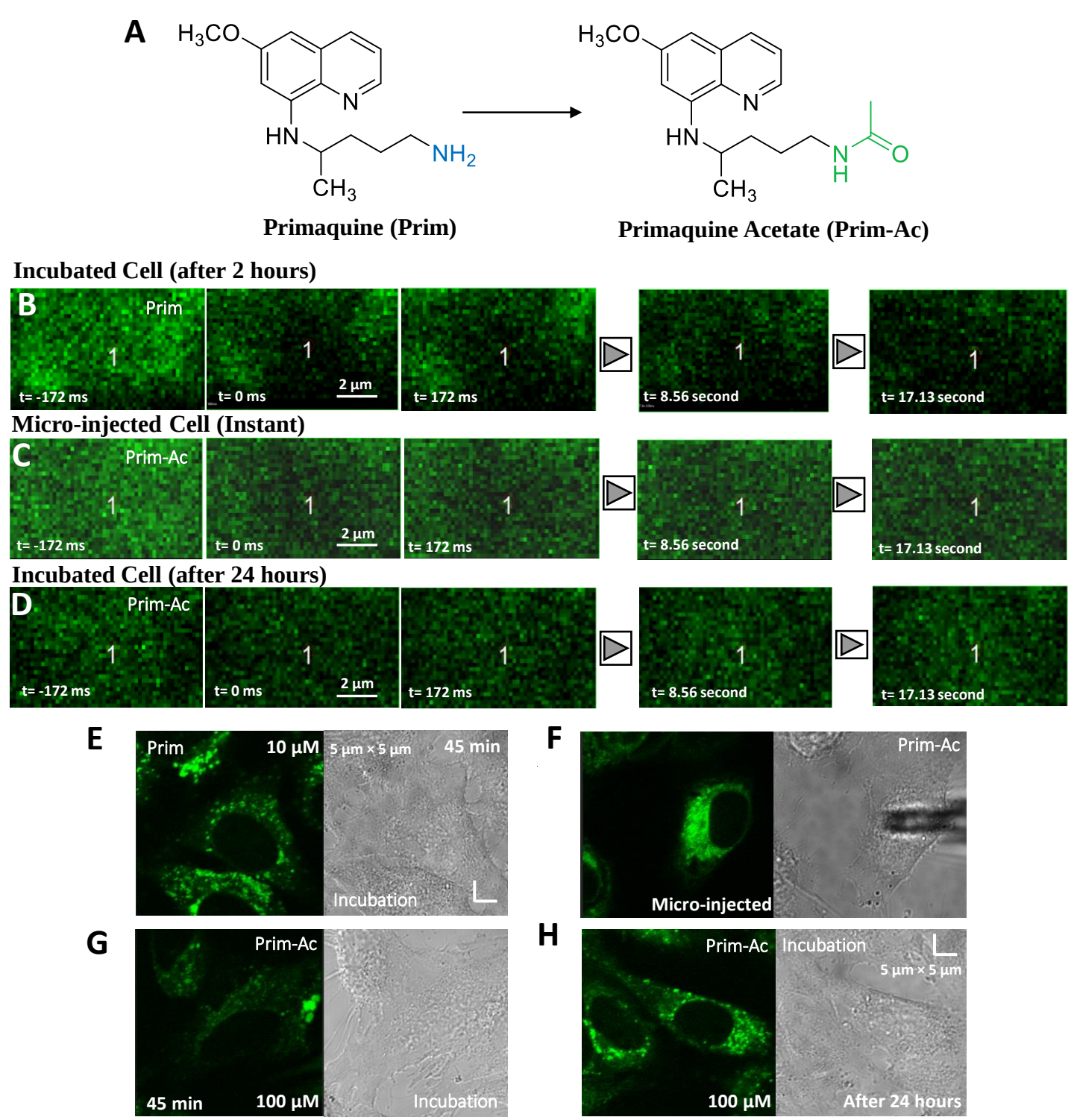

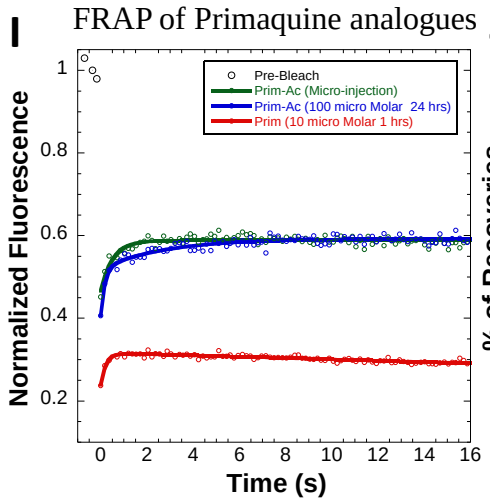

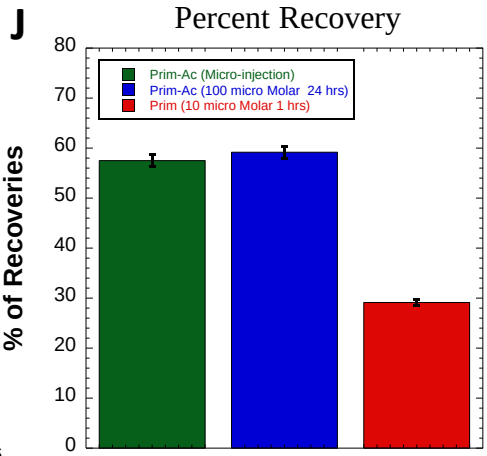

Figure S9: Comparative FRAP of Primaquine analogues inside HeLa cells. (A) Structures of Primaquine analogues with pKa values. Comparative (B-D) XY FRAP micrographs with time lapses in HeLa cell cytoplasm are shown. (E-H) Micrographs of treated HeLa cells either after micro-injection or after drug incubations with Prim or Prim-Ac. Comparative (I) XY-FRAP recovery profiles with fits and (J) percentage of recoveries for Primaquine analogues in HeLa cytoplasm are also shown.

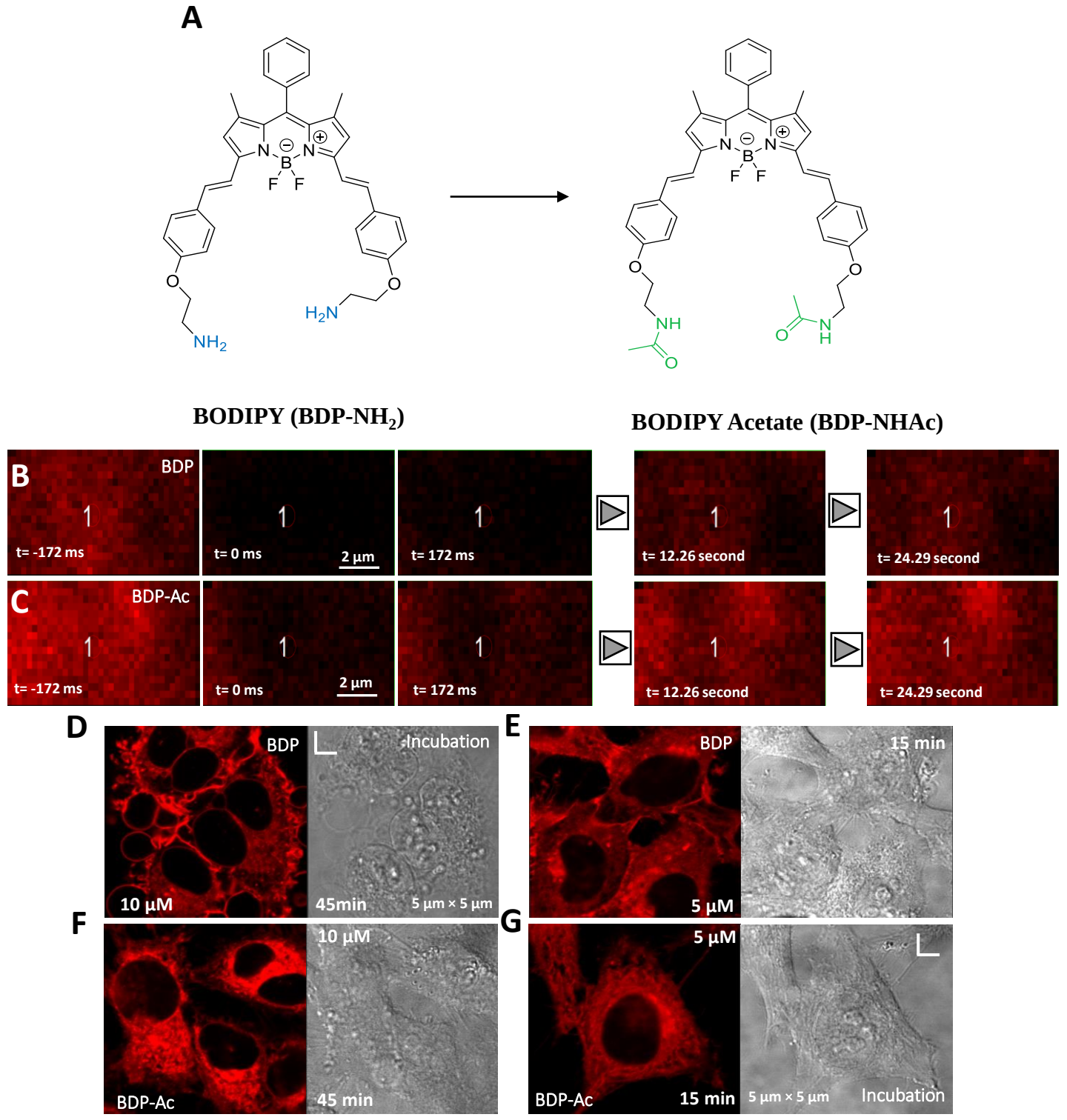

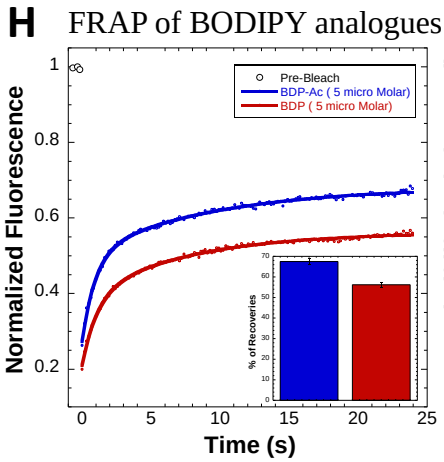

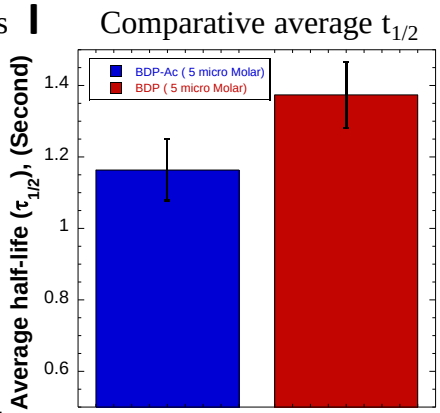

Figure S10: Comparative FRAP of BODIPY analogues inside HeLa cells. (A) Structures of BODIPY analogues. (B-C) Comparative XY FRAP micrographs with time lapses in HeLa cell cytoplasm are shown. (D-G) Micrographs of treated HeLa cells after drug incubations (with BDP/BDP-Ac) and, Comparative (H) XY-FRAP recovery profiles with fits, (I) averaged half-life and percentage of recoveries for BODIPY analogues in HeLa cytoplasm are also shown in the inset (H).

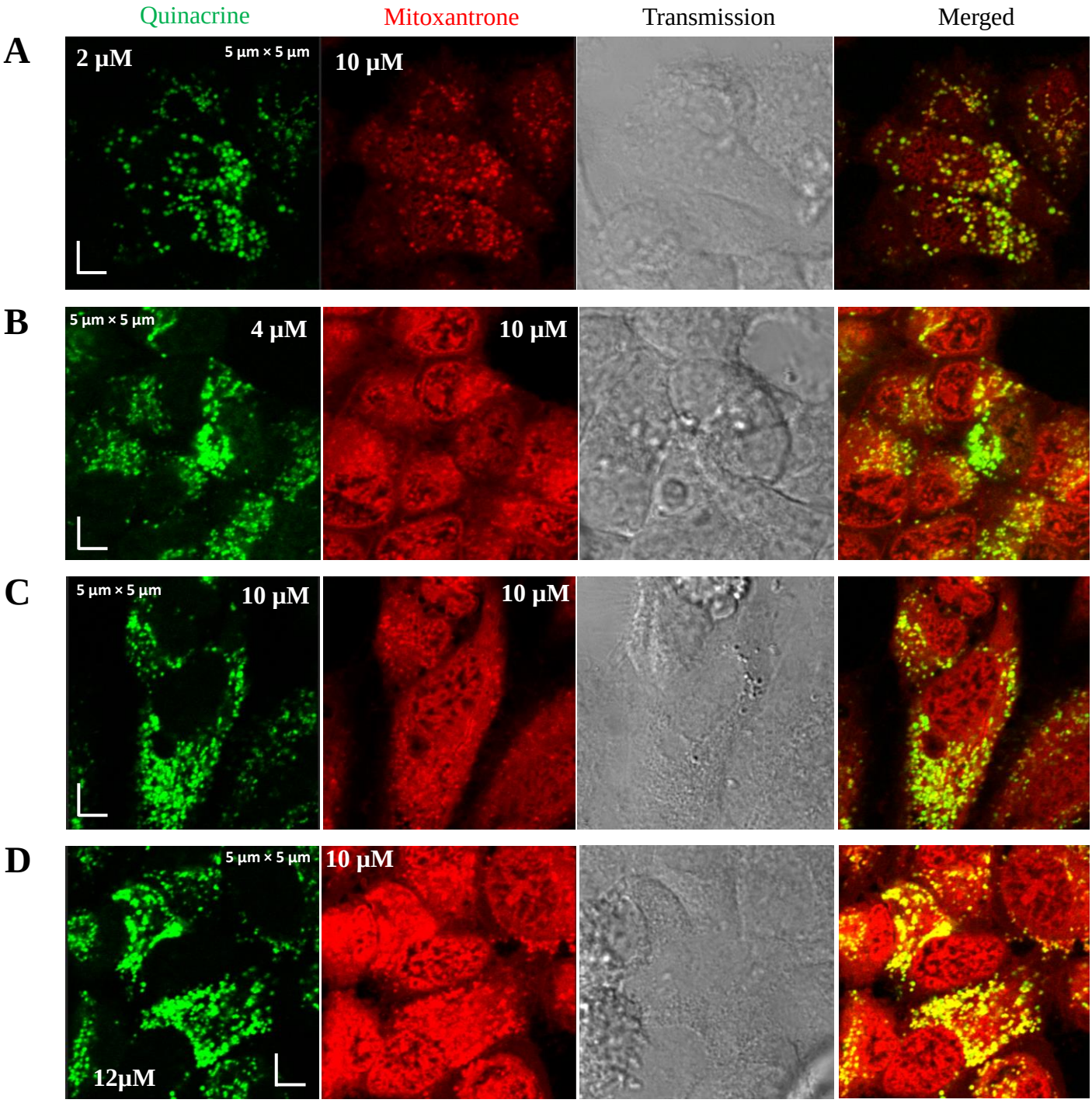

Figure S11: Colocalization of Mitoxantrone and Quinacrine inside HeLa cells. (A-D) Mitoxantrone concentration was kept fixed to 10 µM, whereas Quinacrine concentration was varied from 2-12 µM.

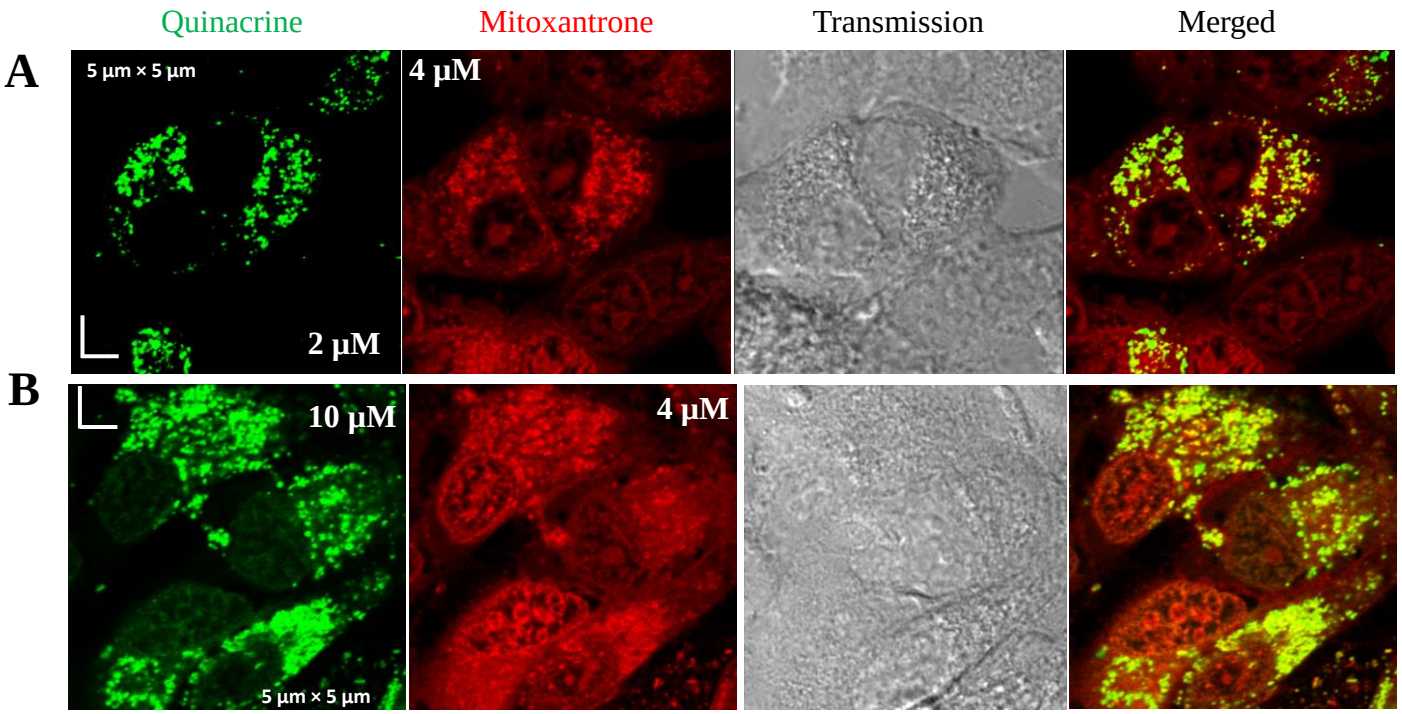

Figure S12: Colocalization of Mitoxantrone and Quinacrine inside HeLa cells. (A, B). Mitoxantrone concentration was kept fixed to 4 µM, whereas Quinacrine concentration were varied from 2-10 µM.

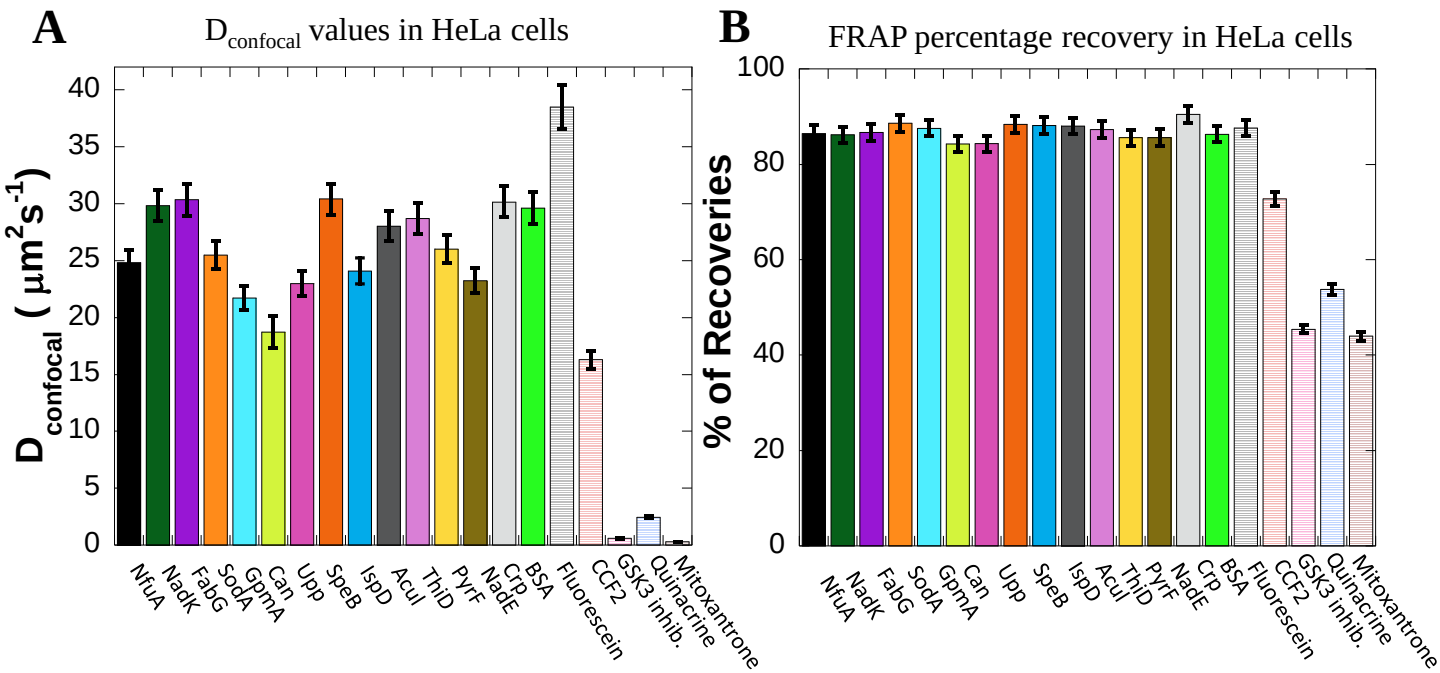

Figure S13: Diffusion coefficients of proteins and small molecules in the HeLa cells. Comparison of (A) diffusion of coefficients and (B) percentage of recoveries of small molecule drugs and different bacterial proteins in HeLa cell cytoplasm are shown.

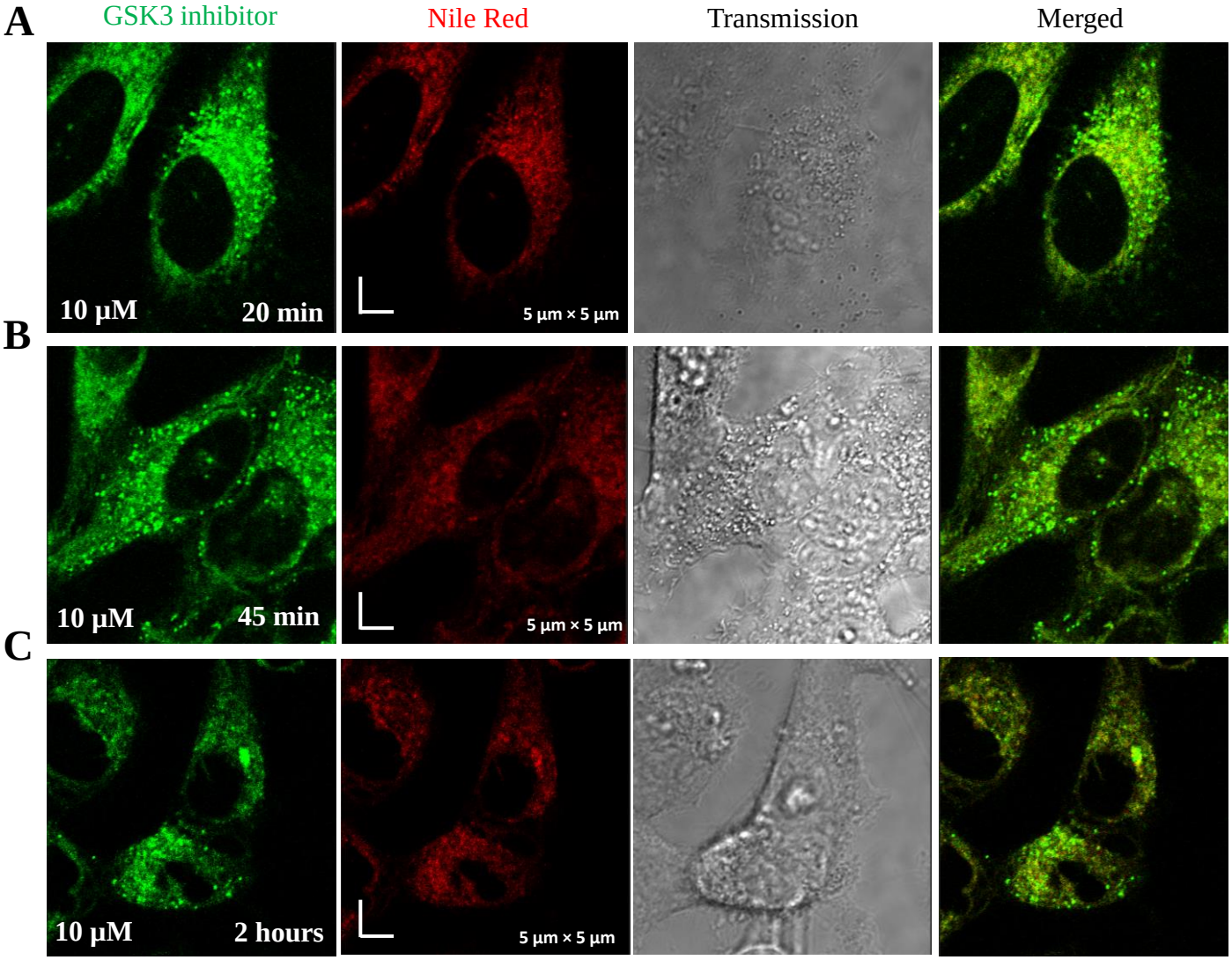

Figure S14: Time dependent colocalization of GSK3 inhibitor and Nile Red inside HeLa cells. Panels (A-C) show Nile red accumulating in lipid droplets, while GSK3 inhibitor does not colocalize.

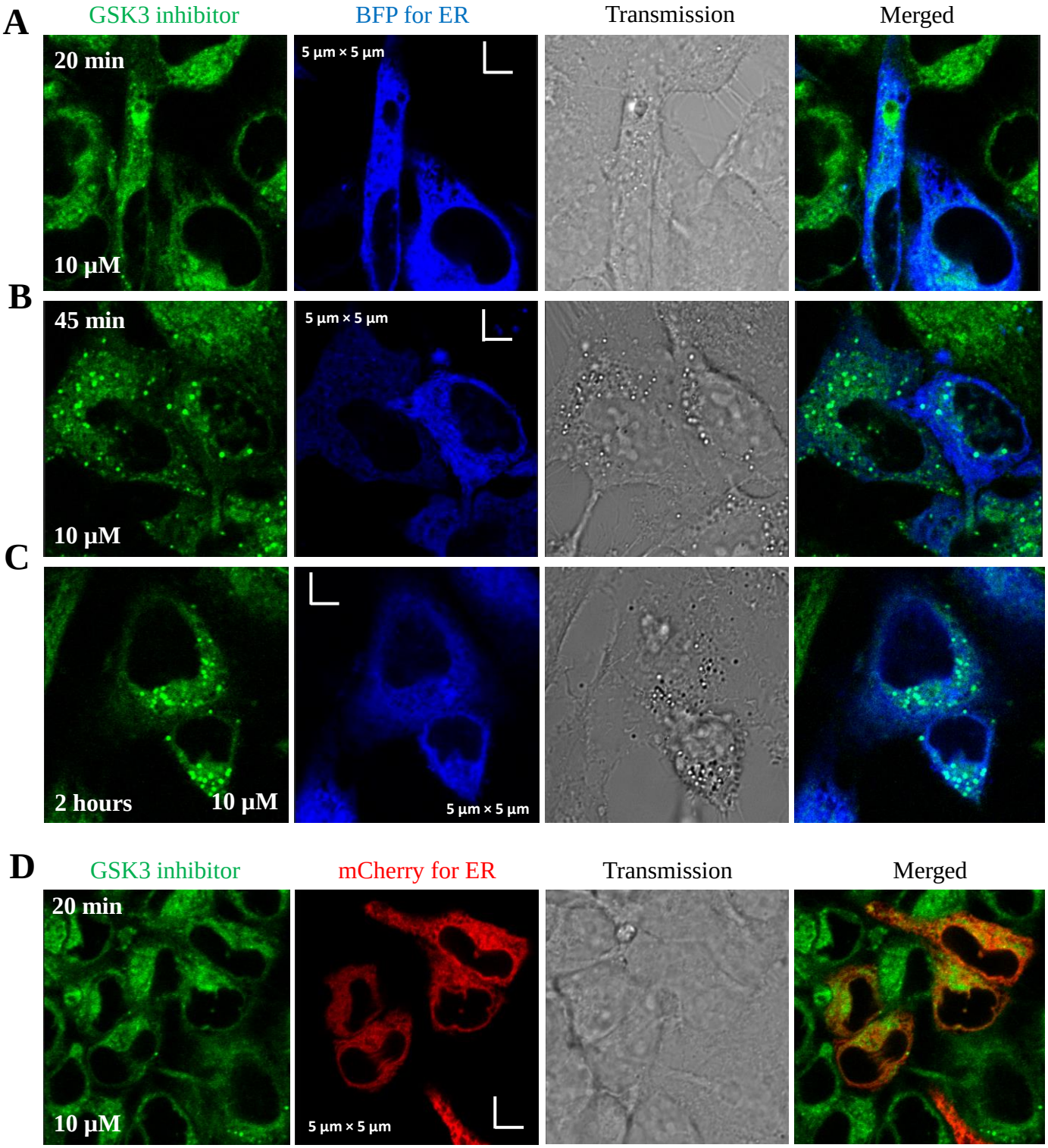

Figure S15: Time dependent colocalization of GSK3 inhibitor and ER marker inside HeLa cells. Panels (A-D) show BFP/mCherry fused antibody marker accumulating in ER, but GSK3 inhibitor does not colocalize. HeLa cells were first transiently transfected with BFP/mCherry fused antibody markers, then treated with GSK3 inhibitor.

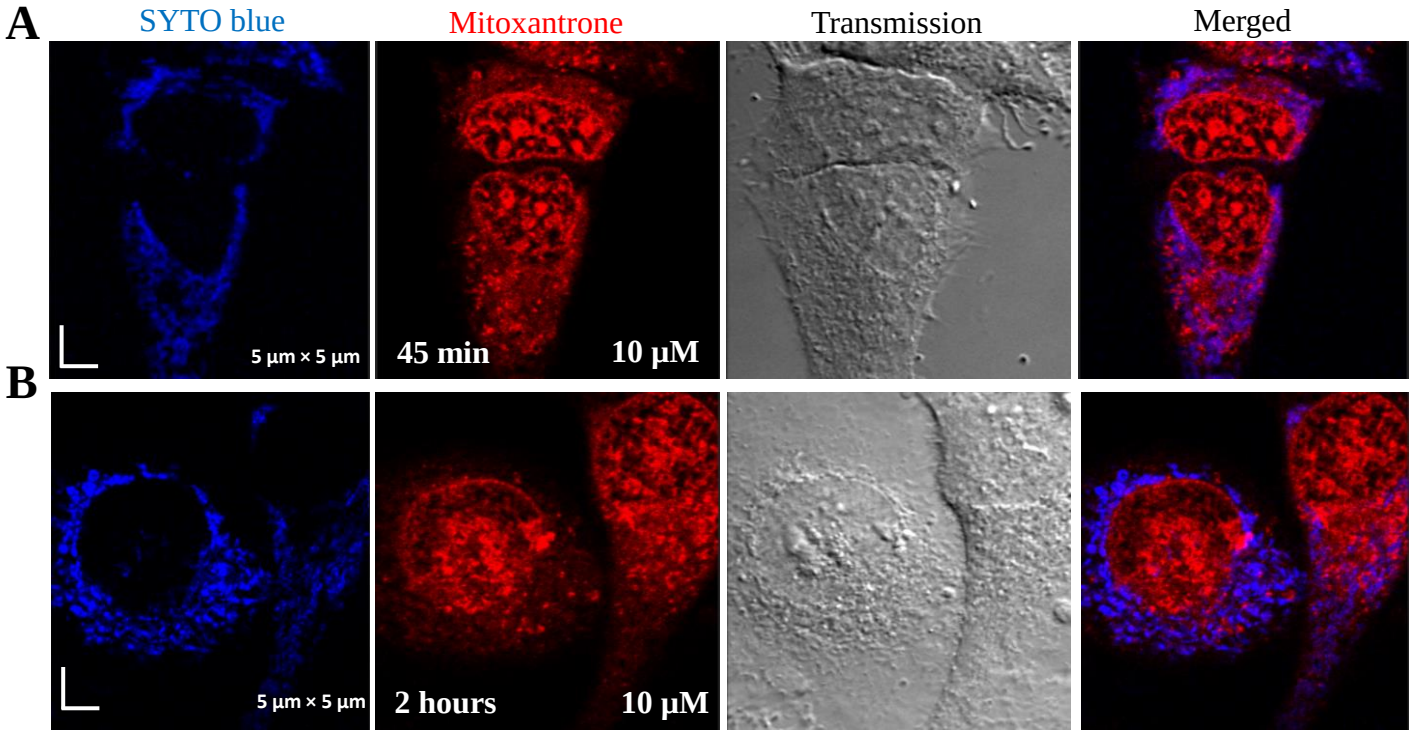

Figure S16: Time dependent colocalization study of Mitoxantrone and SYTO blue marker inside HeLa cells. Panels (A-B) show SYTO blue marker accumulating in nucleic acids, but Mitoxantrone does not colocalized. HeLa cells were first treated with SYTO blue, then treated with Mitoxantrone.

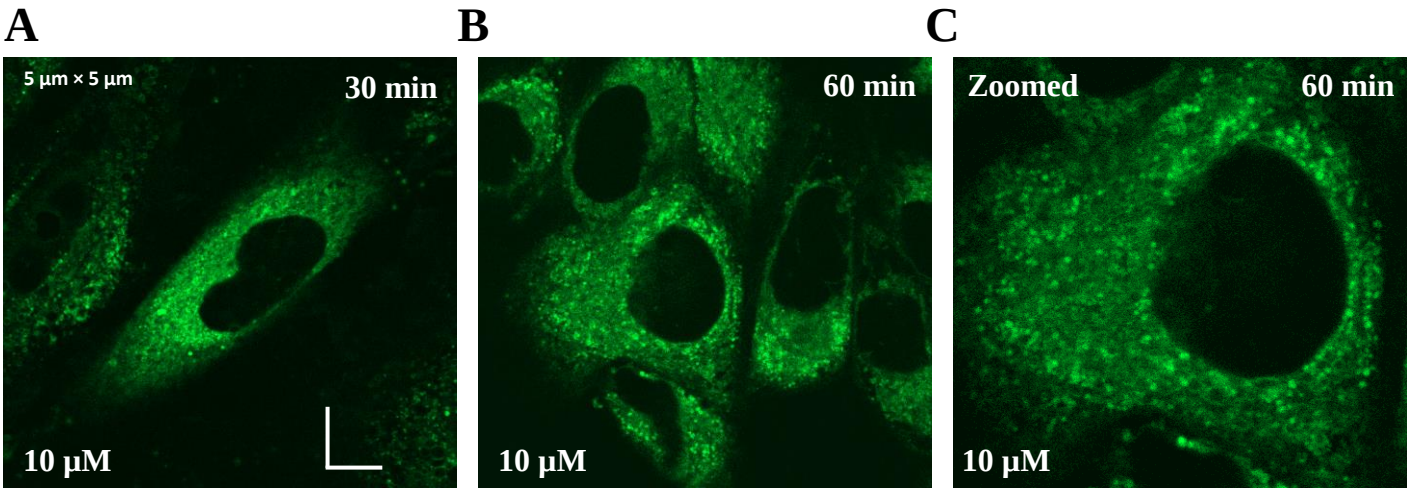

Figure S17: Super resolution images of GSK3 inhibitor treated HeLa cells. Micrographs were taken using a Zeiss LSM900 microscope.

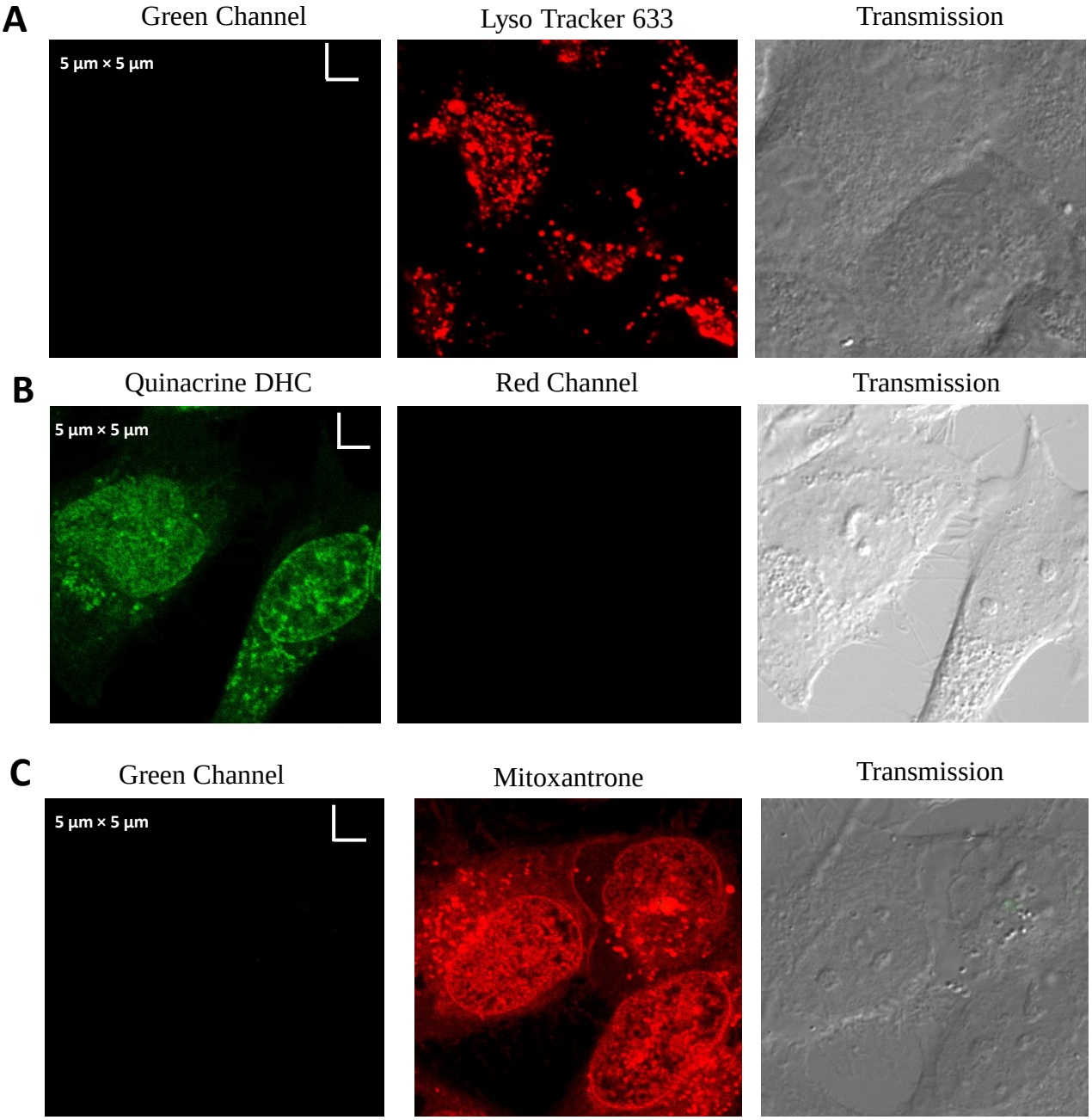

Figure S18: Evaluating channel leakage. Control experiments showing that channel leakage did not occur during colocalization studies. (A) Lyso-Tracker only, (B) Quinacrine only and (C) Mitoxantrone only.

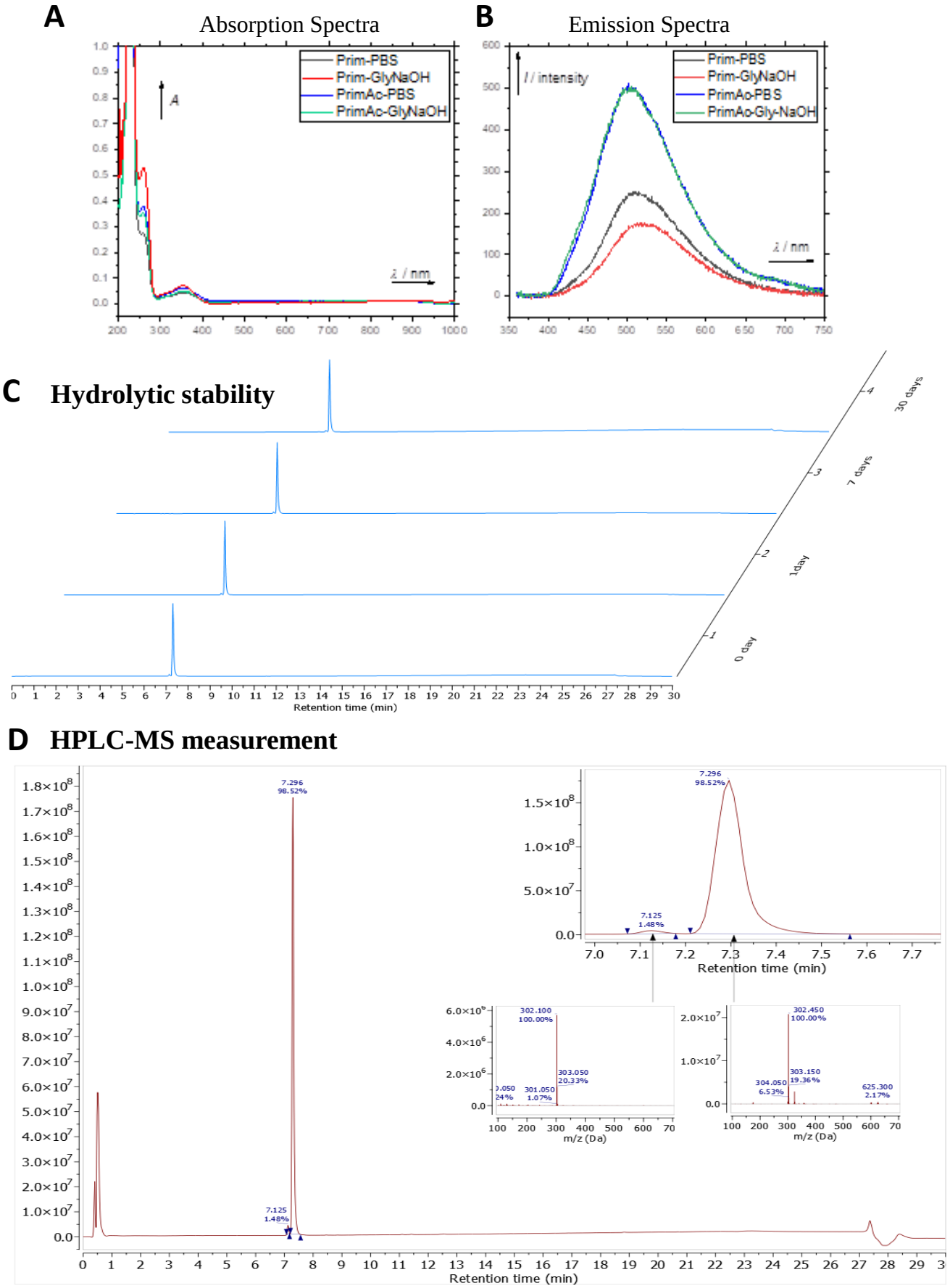

Figure S19: Characterization of Primaquine (Prim) and N-acetylated Primaquine (PrimAc). (A) Absorption (c ≈ 1 · 10-3) and (B) emission (c ≈ 3 · 10-4) spectra. Both experiments were measured in the mixture of 10% DMSO in PBS or in Glycine/NaOH buffer. (C) Measurement of hydrolytic stability by HPLC. (D) HPLC-MS measurement of PrimAc are shown. According to HPLC-MS data the peak at 7.125 corresponds to 302 m/z (ESI +) so as the main peak at 7.296. The molar mass of PrimAc corresponds to the measured value.

A ^{1}H NMR spectrum.

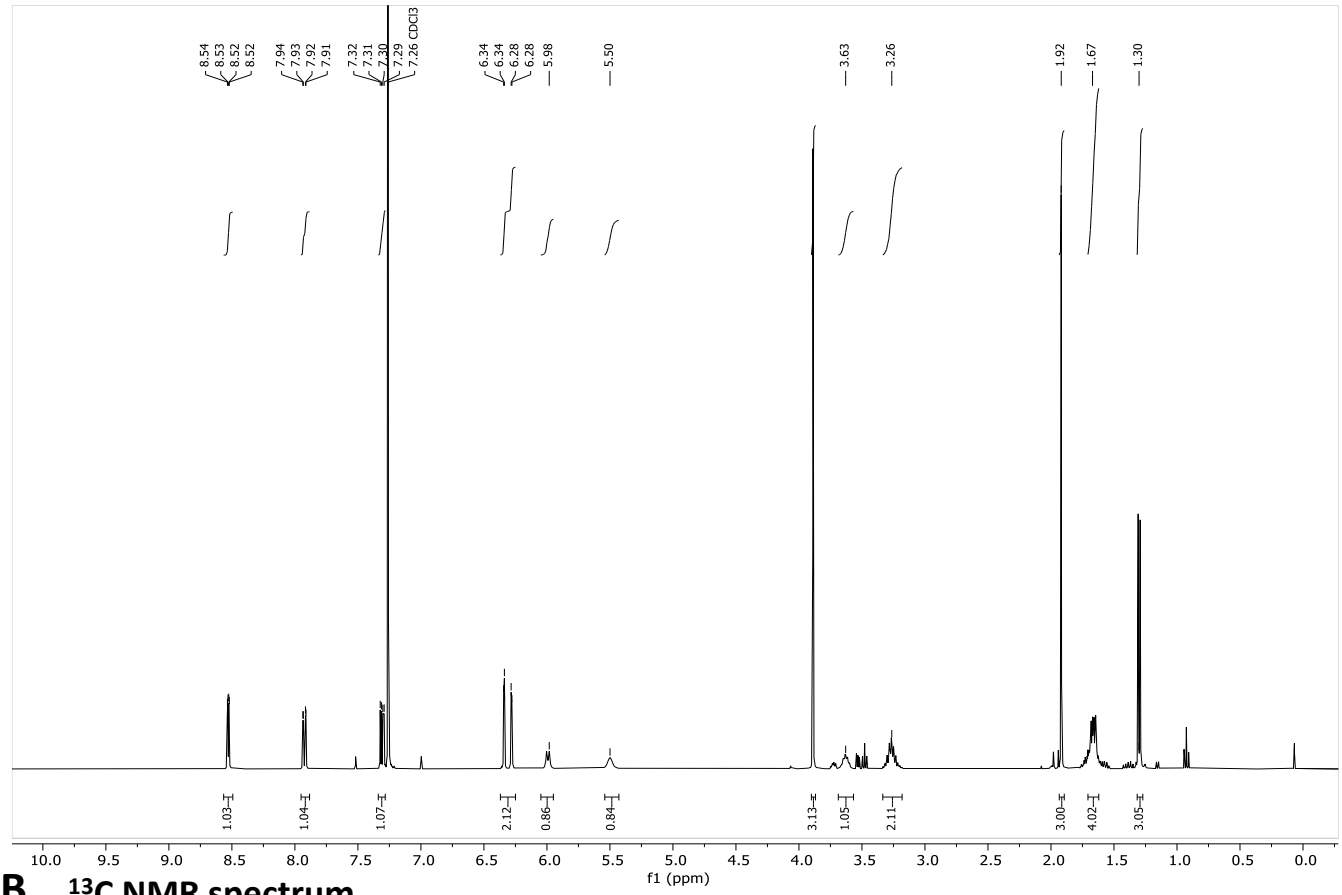

B ^{13}C NMR spectrum

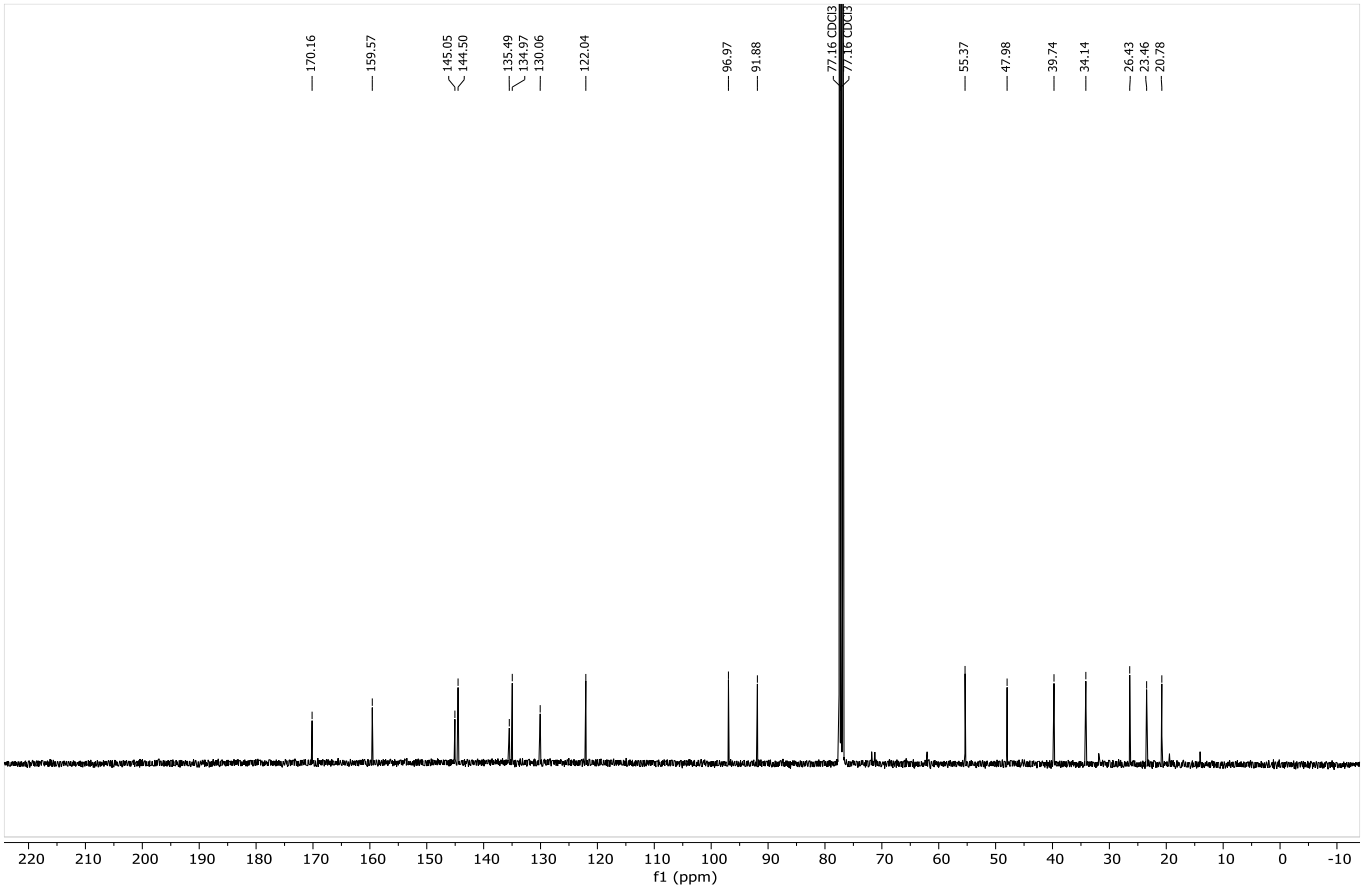

Figure S20: N-acetylated Primaquine. (A) ^{1}H NMR spectrum is shown. The presence of impurities is caused by the degradation in the used solvent. (B) ^{13}C NMR spectrum is shown.

HRMS spectrum

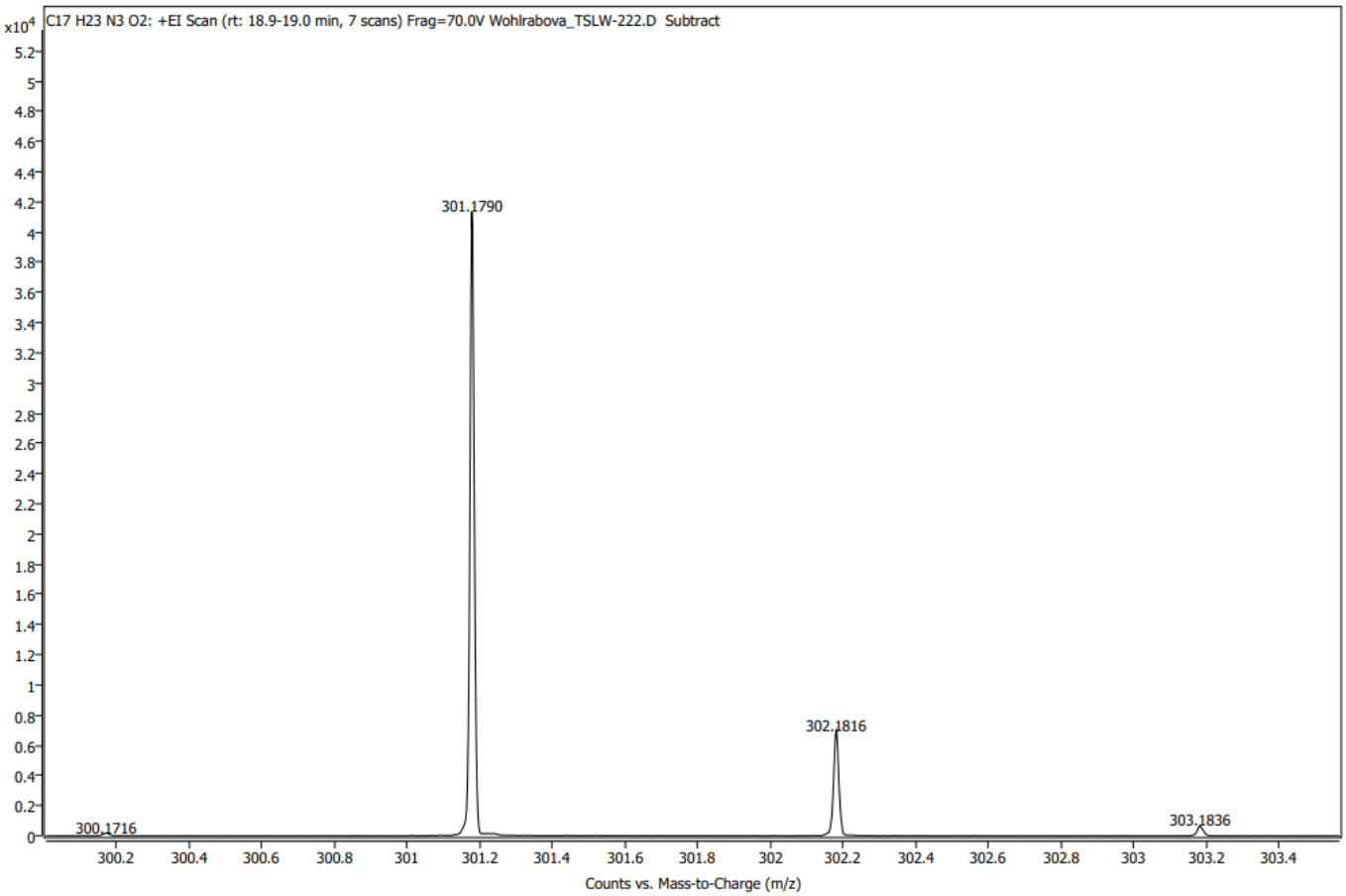

Figure S21: N-acetylated Primaquine. HRMS spectrum (+EI) is shown

BODIPY analogues

A

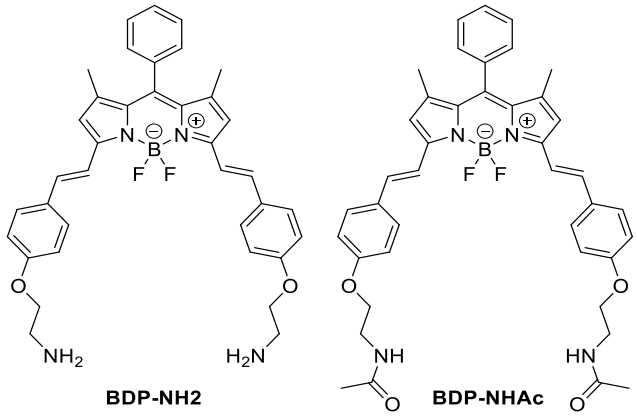

	BDP-NH2	BDP-NHAc
	AP-274-F4-P1	AP-272-P1
	9 mg	3 mg
	DMSO: 649 nm; PBS: 667 nm	DMSO: 649 nm; PBS: 662 nm
	DMSO: 665 nm; PBS: 705 nm	DMSO: 665 nm; PBS: 705 nm
	28 %	40 %
	0.1 %	0.06 %
	0.16 %	0.07 %
	0.15 %	0.08 %
	0.32 %	0.1 %

B **BDP-NH_2**

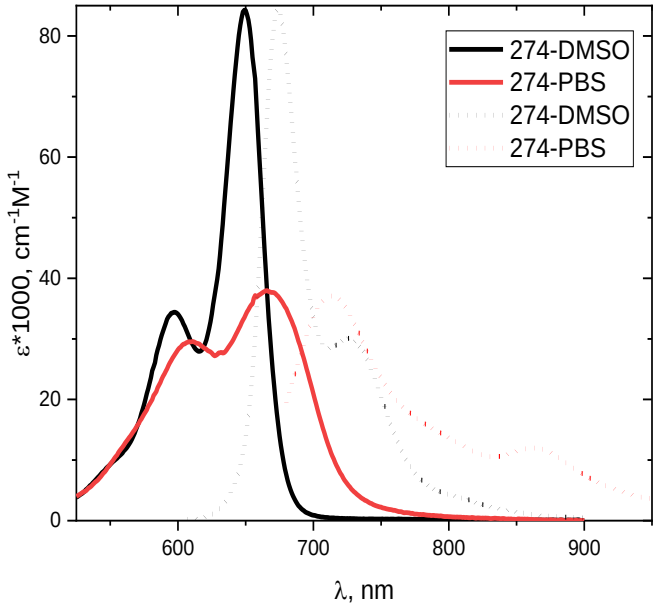

C **BDP-NHAc**

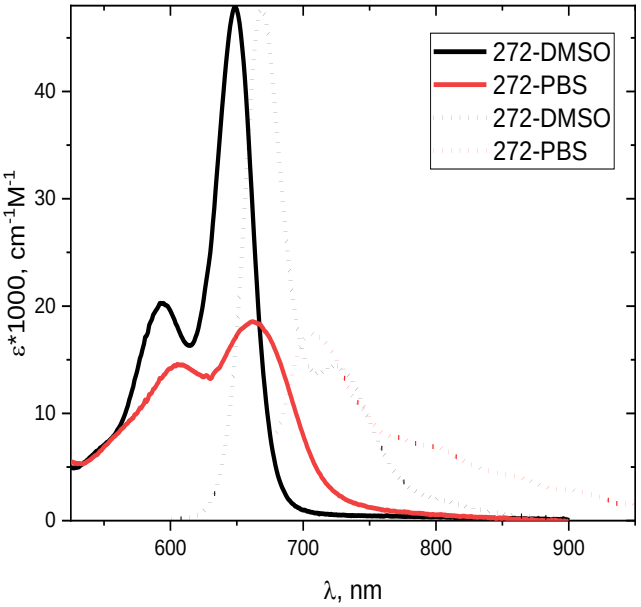

Figure S22: (A) Structure and photo-physical properties of BODIPY analogues. (B) Absorption (full line) and emission spectra (dashed line) of BDP-NH_2 in DMSO (black) and PBS (red) are shown. (C) Absorption (full line) and emission spectra (dashed line) of BDP-NHAc in DMSO (black) and PBS (red) are shown.

A ^{1}H NMR spectrum

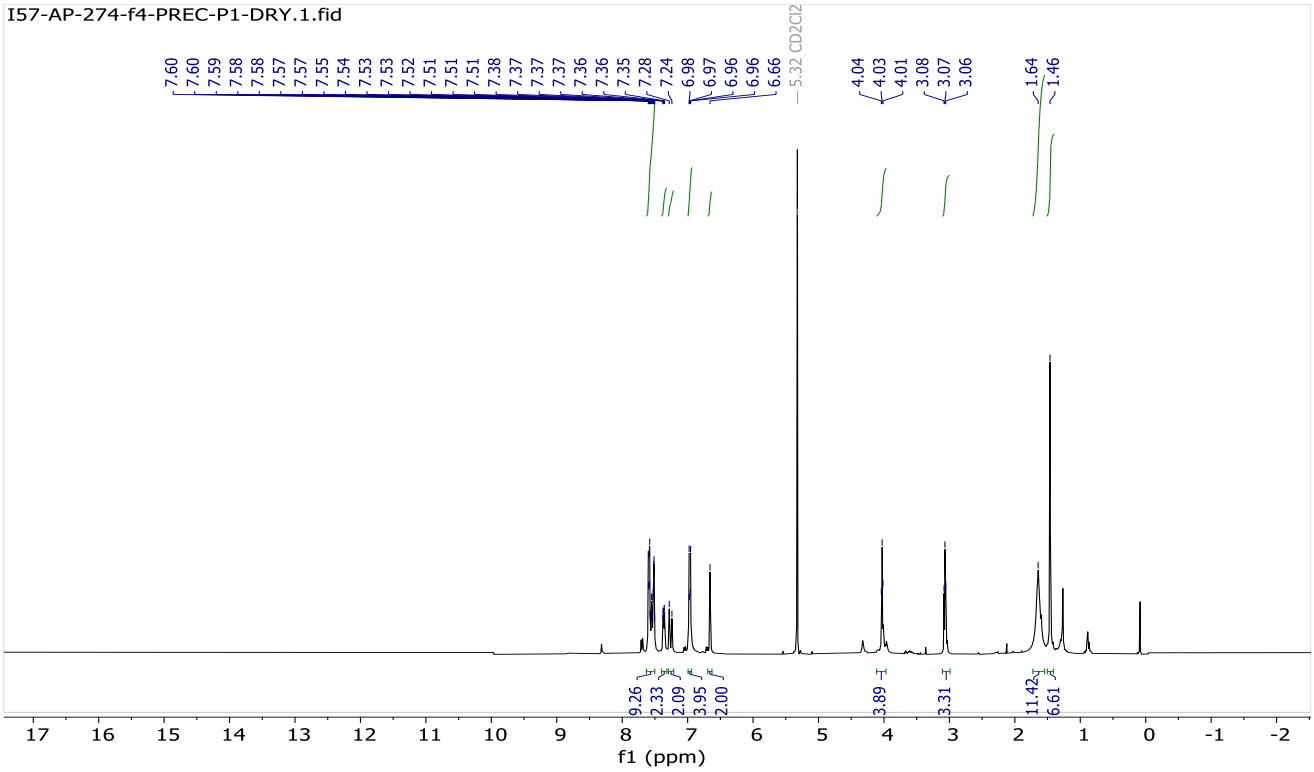

B ^{13}C NMR spectrum

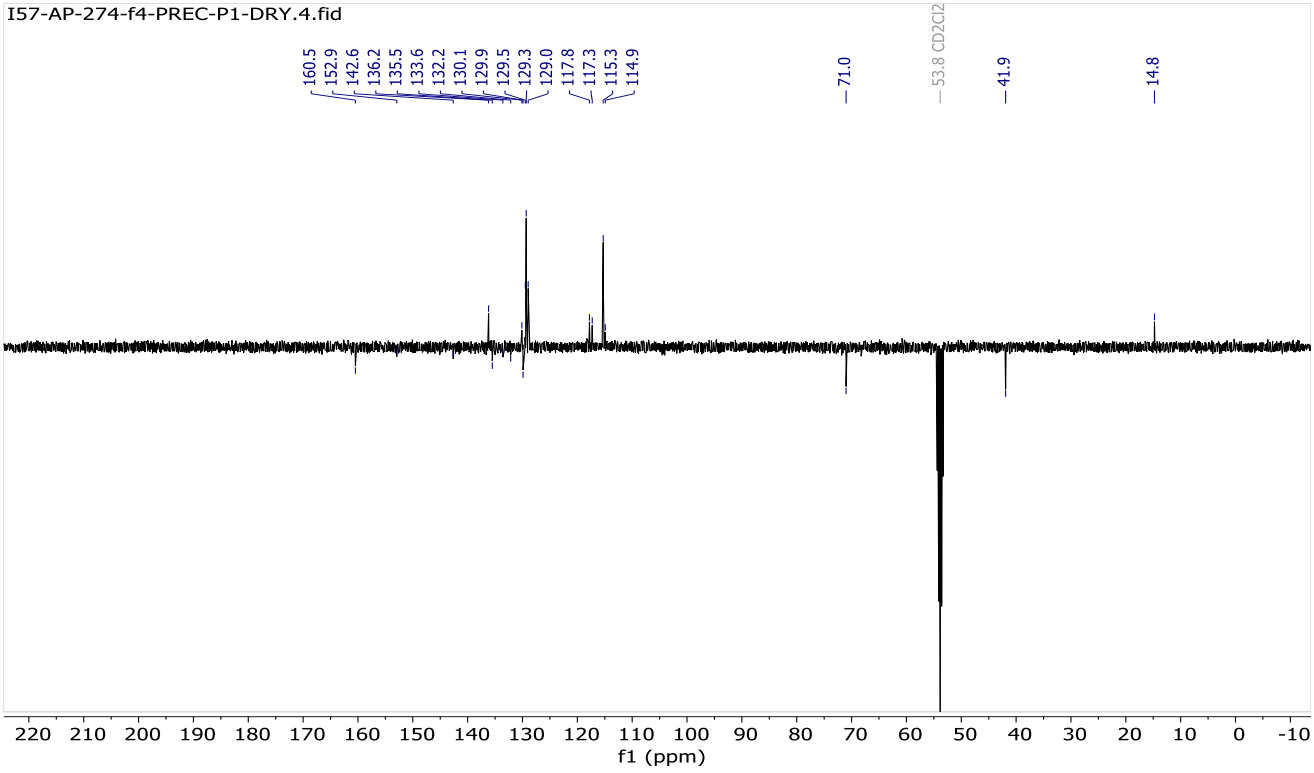

Figure S23: Characterization of BODIPY-NH_2. (A) ^{1}H NMR spectrum and (B) ^{13}C NMR spectrum are shown.

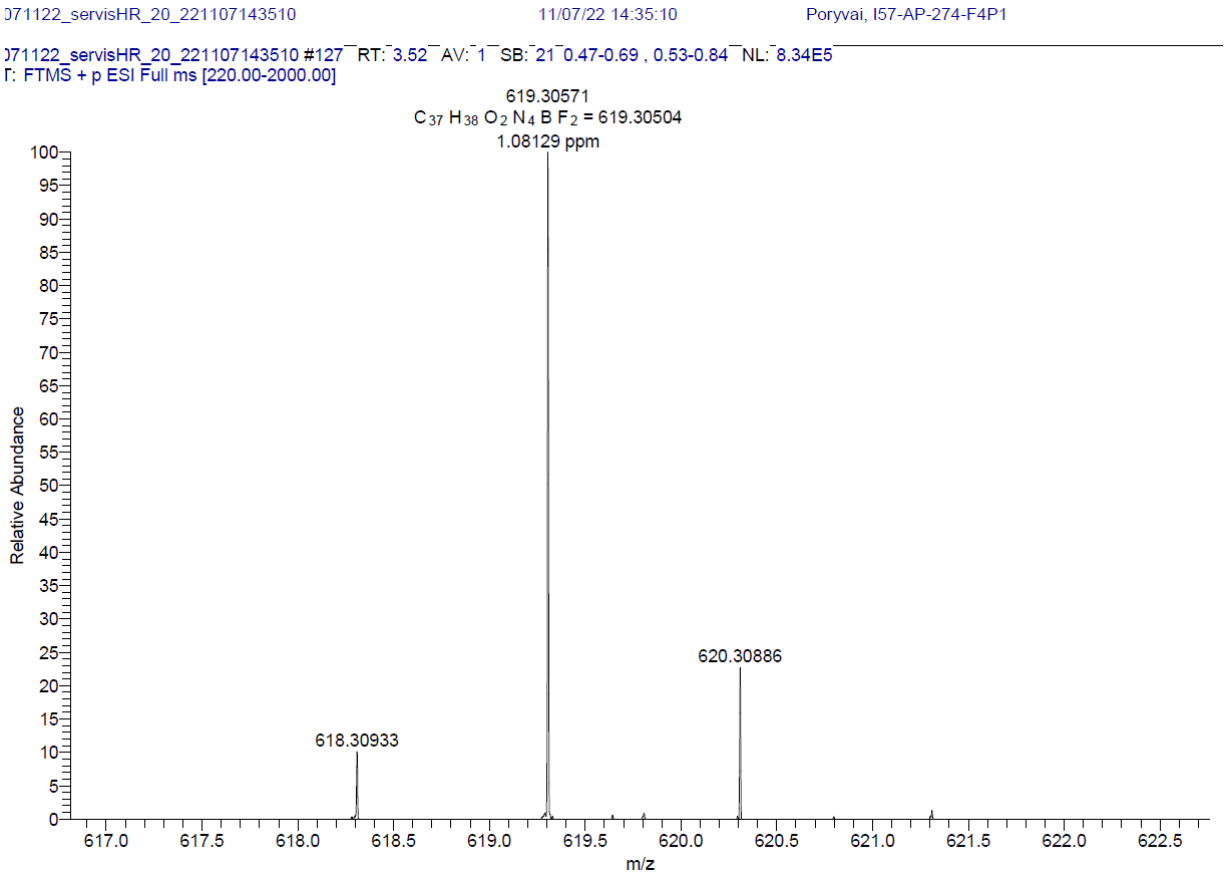

Figure S24: BODIPY-NH_2. HRMS spectrum (+EI) is shown.

A ^{1}H NMR spectrum

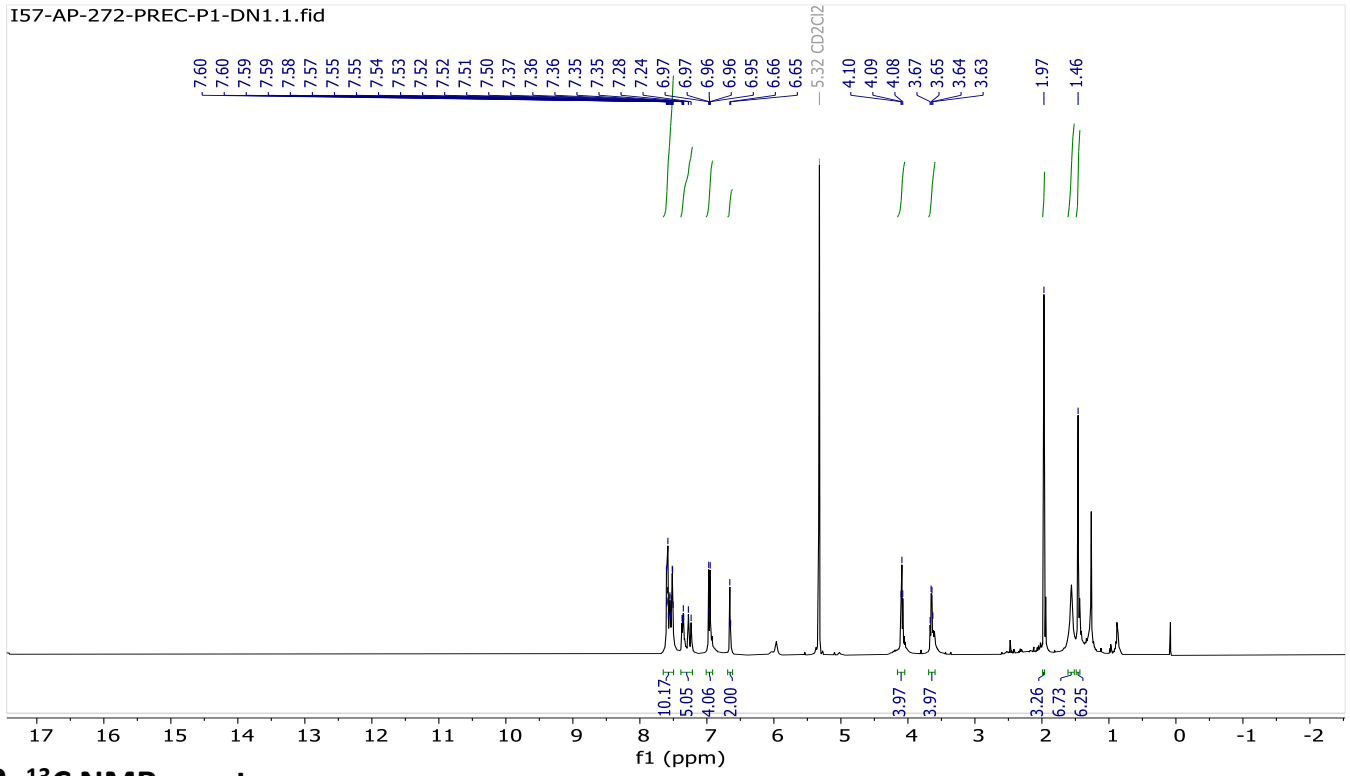

B ^{13}C NMR spectrum

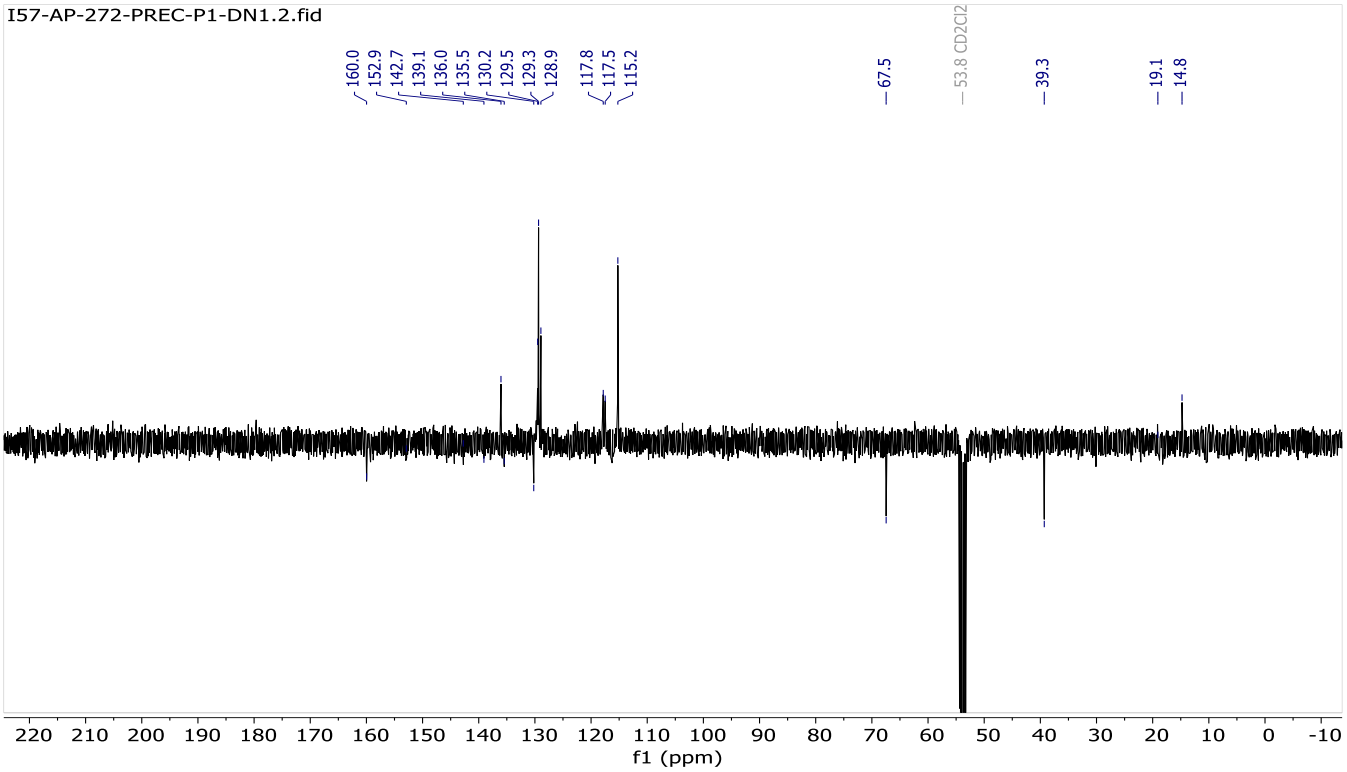

Figure S25: Characterization of BODIPY-NHAc. (A) ^{1}H NMR spectrum and (B) ^{13}C NMR spectrum are shown.

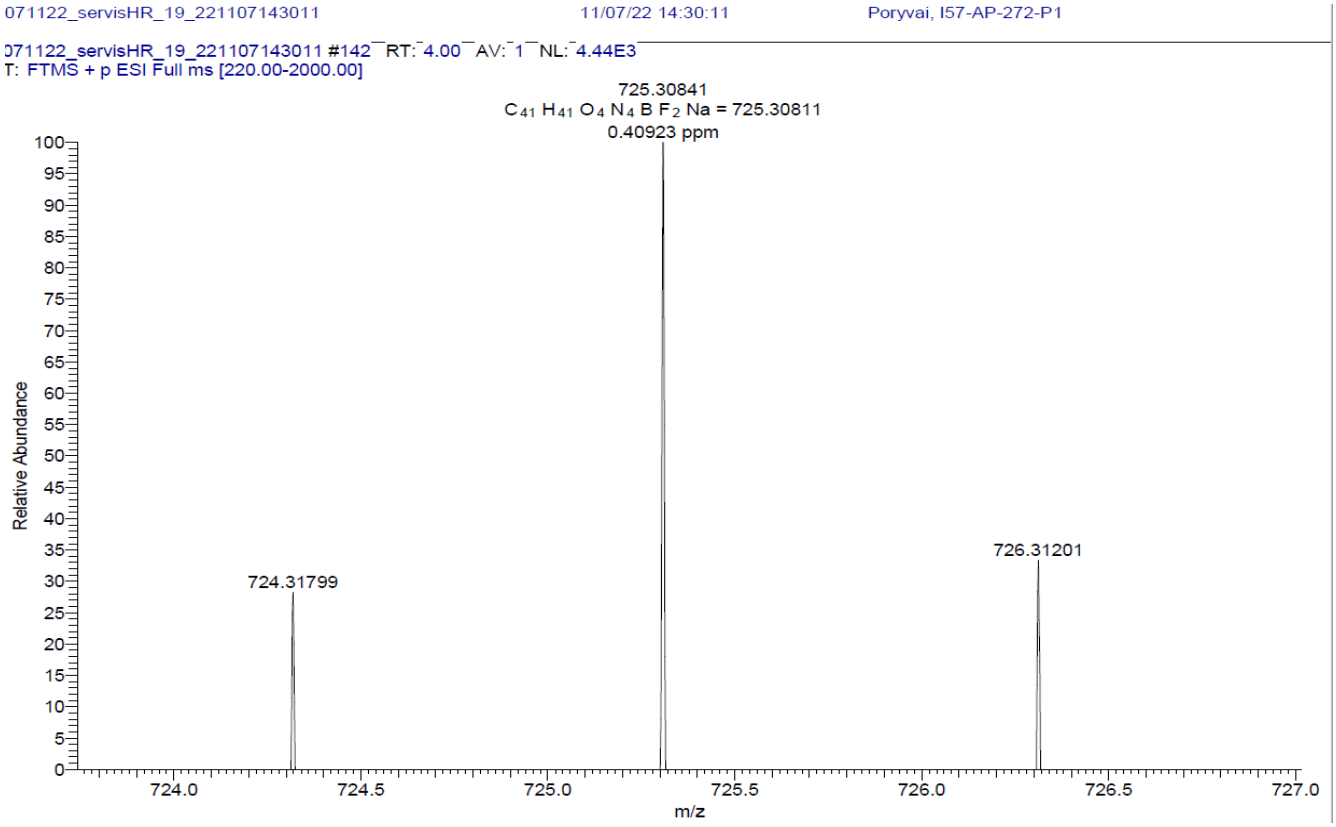

Figure S26: BODIPY-NHAc. HRMS spectrum (+EI) is shown

Supplementary Information

Reversing protonation of weakly basic drugs greatly enhances intracellular diffusion and decreases lysosomal sequestration

Debabrata Dey,[1] Shir Marciano,[1] Anna Poryvai,[2] Ondřej Groborz,[2] Lucie Wohlrábová,[2] Tomáš Slanina[2] and Gideon Schreiber*[,1]

[1]Department of Biomolecular Sciences, Weizmann Institute of Science, Israel

[2]Institute of Organic Chemistry and Biochemistry of the Czech Academy of Sciences, Flemingovo náměstí 542/2, Prague 6, 160 00 Czech Republic

*Corresponding author: gideon.schreiber@weizmann.ac.il

Table S1: Oligomeric state, Isoelectric point and Net charge at pH 7.4

Protein entry	Isoelectric point: pI	Net charge at pH **7.4**: Z	$D_{confocal}$	Oligomeric state
NfuA	4.534	-15.767	24.80	M/D
NadK	6.387	-4.808	29.83	M/D/T
FabG	6.250	-1.66	30.33	D/T/H
E-fts	5.228	-9.527	22.47	M/D
SodA	6.511	-2.481	25.49	D
tpiA	5.688	-7.851	27.94	
GpmA	5.913	-4.262	21.71	D
Can	6.230	-5.908	18.73	T
Upp	5.335	-6.829	22.97	M/D
SpeB	5.160	-14.788	30.39	Tri/H
IspD	6.257	-5.445	24.09	D/T/H
BaeR	5.554	-6.032	21.88	M/D
Acul	5.669	-5.986	28.02	M/D/T/H
PyrF	5.874	-3.9	25.99	M/D
ThiD	5.793	-6.842	28.68	M/D
NadE	5.603	-4.993	23.22	D
CRP	7.979	+1.388	30.14	D/T
DES3im-4rp4	5.041	-5.659	29.41	
DES7im-3rk6	4.599	-10.654	28.83	
6E5C_denovobeta30	6.336	-0.714	30.02	
BSA	4.5–4.8	-15	29.60	M/D

Isoelectric points and net-charges were predicted using Prot Pi. Oligomeric states were taken from [47] from native mass spectrometry measurements.

Table 2. Key resources table

REAGENT or RESOURCE	SOURCE	IDENTIFIER
Chemicals, peptides, and recombinant proteins		
Dulbecco's phosphate-buffered saline (PBS 1X)	Biological Industries	Cat# 02-023-1A
HEPES buffer	Fisher BioReagents	LOT# 170358
DMEM(1X) Gibco	Life Technologies Limited	REF# 41965-039
Fetal Bovine Serum (Gibco)	Life Technologies Limited	REF# 12657-029
Trypsin-EDTA Solution A	Biological Industries	REF# 03-050-1B
Penicillin/ Streptomycin	Biological Industries	REF# 03-031-1B
Sodium Pyruvate Solution	Biological Industries	REF# 03-042-1B
35-mm glass-bottomed dishes	MatTek Corporation	P35G-0-14-C
Pierce™ Dye Removal Columns	Thermo-Fisher scientific	Cat# 22858
Gebaflex tubes 3.5KDa (GeBa)	TIVAN BIOTECH	Cat# MIDI3-100
Capillary Glass Tubing	Warner Instruments	Model No. G120TF-4 203-776-0664
96- well Black F-Bottom Plate	Greiner-bio-one	REF# 655076
Disposable cuvettes	Fisher Scientific	ZEN0040
BSA (Albumin Bovine, fraction V)	MP Biomedicals, LLC	CAS# 9048-46-8
HEWL (Lysozyme from chicken egg white)	Merck	CAS# 12650-88-3
Myoglobin (from equine heart)	Merck	CAS# 100684-32-0
Doxorubicin	AdooQ Bioscience	Cat# A14403
Fluorescein disodium salt	chemcruz	Cat# sc-206026
GSK3 inhibitor SB216763	Abcam	Cat# ab120202
Quinacrine dihydrochloride	Abcam	Cat# ab120749
Primaquine biphosphate	Merck	CAS# 63-45-6
CCF2-FA	Thermo-Fisher Scientific	Cat# K1039a
CF514 Labelling dye	Biotium	CF514 Dye Alternative green fluorescent dye
Amodiaquine	AdooQ Bioscience	Cat# A17660
Sodium Azide	Merck	CAS# 26628-22-8
Mitoxantrone	Abcam	Cat# ab141041
Bafilomycin A1	Abcam	Cat# ab120497
5-amino Fluorescein	Abcam	Cat#ab145305

Characterization of Prmaquine (Prim) and N-acetylated Primaquine (PrimAc).

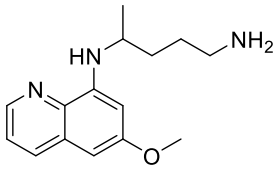

Primaquine (Prim)

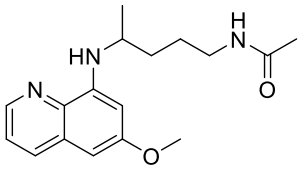

Primaquine acetate (PrimAc)

The absorption and emission spectra of Primaquine analogues are shown in Figure S19 A& B respectively. They were measured in the mixture of 10% DMSO in PBS or in Glycine/NaOH buffer.

Materials & Reagent: Glycine/NaOH (pH = 10) (preparation: 80 mL of distilled water, 0.6 g of glycine, 0.25 g of NaOH, pH adjusted to 10 using 35% HCl, diluted to 100 mL)

Synthesis of PrimAc: To the stirred solution of Primaquine bisphosphate (100 mg, 220 μmol, 1 eq) and TEA (92 μL, 660 μmol, 3 eq) in DMF acetic anhydride (21 μL, 220 μmol, 1 eq) was added at RT. Reaction mixture was stirred for 5 minutes and the reaction mixture was diluted with dichloromethane (50 mL) and extracted 2x with water. Water phase was extracted with 20 mL of DCM and combined organic layers were extracted with brine. The organic phase was evaporated to the volume of approximately 1 mL and the solution was liquid loaded to the column. Gradient chromatography was done using cyclohexane, ethyl acetate and methanol (grad.: 100% cyclohexane – 30% cyclohexane, 60% ethyl acetate, 10% methanol). The chromatography was repeated to obtain the target compound as yellowish oil in 94% yield and 98.5% purity.

^{1}H NMR (401 MHz, CDCl3) δ 8.53 (dd, *J* = 4.2, 1.6 Hz, 1H), 7.92 (dd, *J* = 8.3, 1.6 Hz, 1H), 7.31 (dd, *J* = 8.2, 4.2 Hz, 1H), 6.34 (d, *J* = 2.5 Hz, 1H), 6.28 (dd, *J* = 2.6, 0.6 Hz, 1H), 5.99 (d, *J* = 8.4 Hz, 1H), 5.50 (s, 1H), 3.69 – 3.58 (m, 1H), 3.36 – 3.18 (m, 2H), 1.92 (s, 3H), 1.72 – 1.63 (m, 5H), 1.30 (d, *J* = 6.4 Hz, 3H). **^{13}C NMR** (101 MHz, CDCl3) δ 170.03, 159.45, 144.92, 144.37, 135.36, 134.84, 121.91, 96.84, 91.75, 55.24, 47.85, 39.61, 34.01, 26.30, 23.33, 20.65. (Figure S20 A&B). HRMS spectrum of Primaquine-Ac is shown in Figure S21.

Hydrolytic experiment: The compound PrimAc (1 mg) was dissolved in 20 μL DMSO and diluted with 1.98 ml 0.1M PBS. The solution was measured by HPLC-MS (0-day, 1 day, 7 days, 1 month). The sample was stored in the dark at 25 °C between measurements. (Figure S19 C&D)

Characterization of BODIPY-NH_2 (BDP-NH_2) and BODIPY-NHAc (BDP-NHAc).

The Structures and photo-physical properties of BODIPY analogues are shown in Figure S22A. The absorption and emission spectra of BODIPY-NH_2 and BODIPY-NHAc in PBS/DMSO are shown in Figures S22B,C, respectively.

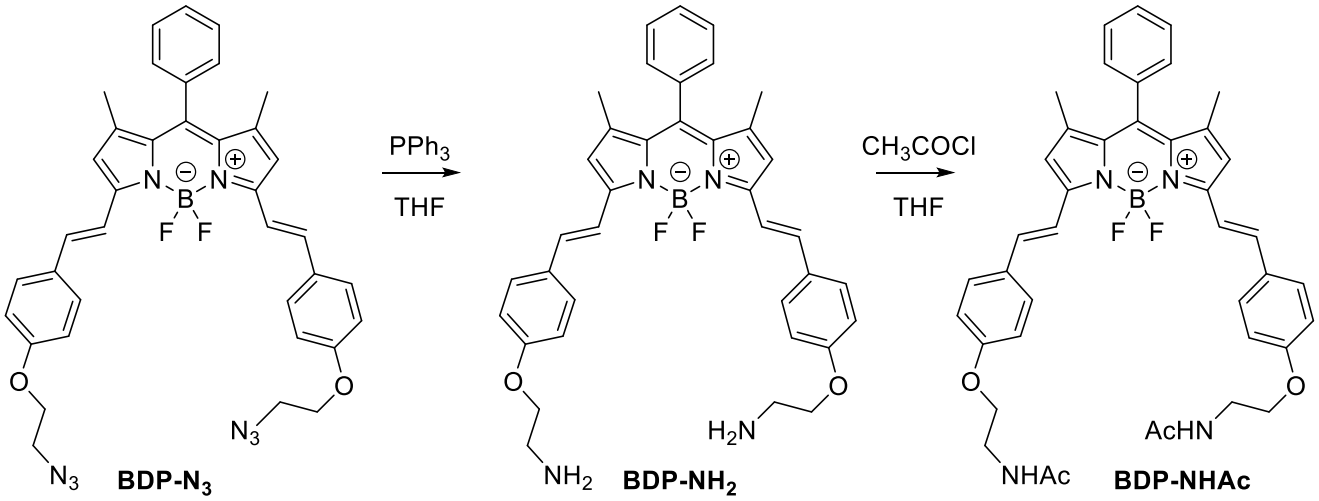

BDP-NH_2: To a solution of a starting **BDP-N_3** (60 mg, 0.1 mmol, 1 eq.) and PPh_3 (47 mg, 0.2 mmol, 2 eq.) in THF (8 mL) water (1 mL) was added. The reaction mixture was stirred for 24 h and transferred on 20 g of silica. First fractions were eluted using a MeOH/DCM, 6/1 mixture followed by elution of the product using MeOH/DCM/NH_3 aq, 90/7/3, mixture. Organic solvents were removed under vacuum and an aqueous layer was extracted using DCM. The final crude product was reprecipitated from DCM using pentane, yielding blue crystals (34 mg, 61 % yield).

^{1}H NMR (401 MHz, CD_2Cl_2) δ 7.64 – 7.49 (m, 11H), 7.26 (d, *J* = 16.3 Hz, 2H), 7.01 – 6.92 (m, 4H), 6.66 (s, 2H), 4.03 (t, *J* = 5.2 Hz, 4H), 3.07 (t, *J* = 5.2 Hz, 4H), 1.64 (s, 4H), 1.46 (s, 6H). ^{13}C NMR (101 MHz, CD_2Cl_2) δ 160.5, 152.9, 142.6, 136.2, 135.5, 133.6, 132.2, 130.1, 129.9, 129.5, 129.3, 129.0, 117.8, 117.3, 115.3, 114.9, 71.0, 41.9, 14.8. HR-MS (ESI+), m/z: [M+H]+, calcd for $[C_{37}H_{38}O_2N_4BF_2]^+$ 619.30571, found 619.30504. ^{1}H NMR and ^{13}C NMR of **BODIPY-NH_2** are shown Figures S23A,B, respectively. HRMS spectrum of **BODIPY-NH_2** is shown in Figure S24.

BDP-NHAc: To a solution of **BDP-NH_2** (5 mg, 0.008 mmol, 1 eq.) in THF (2.0 ml), Et_3N (15 mg, 0.14 mmol, 17 eq.) and CH_3COCl (11 mg, 0.15 mmol, 18 eq) were added. The reaction mixture was stirred at r.t. for 2 h. Water was added and a product was extracted using DCM. The solvent was removed under

reduced pressure and the crude product was 3 times reprecipitated from DCM using pentane, yielding blue crystals (4.5 mg, 79 %).

^{1}H NMR (401 MHz, CD_2Cl_2) δ 7.78 – 7.46 (m, 10H), 7.40 – 7.31 (m, 3H), 7.26 (d, *J* = 16.3 Hz, 2H), 7.01 – 6.89 (m, 4H), 6.65 (s, 2H), 4.09 (t, *J* = 5.1 Hz, 4H), 3.65 (q, *J* = 5.4 Hz, 4H), 1.97 (s, 3H), 1.46 (s, 6H). ^{13}C NMR (101 MHz, $CDCl_3$) δ 160.0 (C), 152.9 (C), 142.7 (C), 139.1 (C), 136.0 (CH), 135.5 (C), 130.2 (C), 129.5 (CH), 129.3 (CH), 128.9 (CH), 117.8 (CH), 117.5 (CH), 115.2 (CH), 67.5 (CH_2), 39.3 (CH_2), 19.1 (CH_3), 14.8 (CH_3). HR-MS (ESI+), m/z: [M+H]+, calcd for $[C_{41}H_{41}O_4N_4BF_2Na]^+$ 725.30841, found 725.30811.

^{1}H NMR and ^{13}C NMR of **BODIPY-NHAc** are shown Figures S25A,B respectively. HRMS spectrum of **BODIPY-NHAc** is shown in Figure S26.